AN ANALYSIS AND IMPROVEMENT OF BRUSHLESS DC MOTOR CONTROL SYSTEM

A Thesis
Submitted to the Graduate Faculty
of the
North Dakota State University
of Agriculture and Applied Science

By

Md Yiasin Sumon

In Partial Fulfillment
of the Degree of
MASTER OF SCIENCE

Major Department:
Electrical and Computer Engineering

September 2013

Fargo, North Dakota

North Dakota State University
Graduate School

AN IMPROVEMENT OF BRUSHLESS DC MOTOR CONTROL SYSTEM

By

Md Yiasin Sumon

The Supervisory Committee certifies that this ***disquisition*** complies with North Dakota State University's regulations and meets the accepted standards for the degree of

MASTER OF SCIENCE

SUPERVISORY COMMITTEE:

Subbaraya Yuvarajan

Chair

Rajesh Kavasseri

Shafiqur Rahman

Approval:

09/19/2013
Date

Scott Smith
Department Chair

ABSTRACT

Trapezoidal Back-EMF (Brushless DC) motors are gaining increasing importance in automotive industries, HVAC applications, home appliances etc. Traditionally, Brushless DC motors are commutated electronically using position sensors. In these systems, mechanical or electromagnetic sensors are used. In sensorless control, rotor back EMF detection is the most popular technique for speed and position control. Detection of back EMF by novel speed independent commutation function is a very well researched topic that has overcome most of the problems of traditional back EMF detection scheme.

In this thesis, a thorough study and speed control scheme for Brushless DC motors using position sensor is presented along with simulation and experimental results. An improved sensorless scheme based on speed independent commutation and state observer based back EMF sensing is analyzed. Both methods use hysteresis control for the current loop and a PI controller for the speed loop to reduce steady state speed error.

ACKNOWLEDGEMENTS

I am greatly indebted to my advisor **Dr. Subbaraya Yuvarajan** for his continuous help, guidance and support that he has provided throughout the years that I have been in the Power Electronics and Drives Lab of North Dakota State University. His attitude towards research, solving problems, inspiring thinking and knowledge he shared are invaluable for my professional career in future and in going through the rest of my life.

I would also like to give my heartiest thanks to **Dr. Rajesh Kavasseri** for being a great mentor of mine throughout my masters program. His professional perspective in managing a project and conducting research will be very important in my life to follow. I want to thank **Dr. Shafiqur Rahman** for his time and efforts he spent as my committee member.

I am grateful to my friend **Jeff Erickson** for his help and time during my stay here at the Power lab. Without his invaluable help about the technical resources it would have been very tough to conduct my research. I also want to thank **Priscilla Schlenker** and **Laura Dallmann** for helping me whenever I needed. I am grateful to the department of Electrical and Computer Engineering for providing me financial assistance during my graduate study. I would like to thank all my friends and colleagues in Power Electronics and Drives Lab for being with me in hard times.

Finally, I am greatly indebted to my beloved parents and family members, especially my father who could not see me completing my journey through my master's program, without the encouragement and inspiration of whom I would never be able to start and complete my work.

TABLE OF CONTENTS

LIST OF TABLES

LIST OF FIGURES

CHAPTER 1. INTRODUCTION

1.1. Background

Improvement in energy efficiency has been one of the most challenging tasks in new generation electrical industry over the last decade. Economic constraints and new standards by government are putting increasingly stringent requirements on different electrical systems. New generation equipment, components and systems must have higher energy efficiency with reduced operating cost. Electric drive industry is one of those important industries where there are a lot of opportunities for improving energy efficiency and reducing electromagnetic interference. Among different electric drives, permanent magnet Brushless DC (BLDC) motor drive has gained increasing importance in the last couple of decades especially for small horse-power motors due to its high efficiency, compact form, reliability and easier control mechanism compared to permanent magnet AC motor drives. The continuous improvement in the use of microprocessors, power semiconductor devices, speed drive mechanisms and the cost reduction of BLDC has brought attractive solutions for BLDC controlled systems at reduced cost.

Brushed DC motors have the advantages of simple solution and reduced complexity in a variable speed drive. But although the drive for conventional brushed DC motor is simple and efficient, its application has been limited due to sparking, wearing and tearing of brushes which requires frequent maintenance resulting in an increased cost [1]. Moreover, the sparking increases the temperature which is also a concern. All these limitations can be overcome with the use of BLDC drives. Conventionally, brushless DC motors are known as trapezoidal back-EMF permanent magnet DC motors.

One of the fastest growing applications of electric drives in the US and all over the world is in household appliances [2]. These appliances include washers, dryers, air conditioners, freezers, vacuum cleaners etc. The amount of energy consumption by these appliances is increasing drastically and constitutes a major source of utility energy consumption. Conventionally, these appliances used to be run employing classical motor techniques, such as single phase ac motor running at constant speed which is inefficient in terms of energy and cost. The increasing amount of energy waste and government enforcement on saving energy have imposed added importance on developing and using efficient variable speed motor drives. Since BLDC motors offer low cost solutions for these applications, the improvement of BLDC drives is a major thrust in today's industries. At the same time, HVAC and automotive industries are experiencing rapid growth especially in the last decade. Hybrid and electric cars have already made their way. Electronically controlled motor systems are integral parts of automotive industries these days, a lot of which are of BLDC controlled [3]. Low cost solutions provided by BLDC motors are expected to make bigger contributions towards this growth.

1.2. Trapezoidal Back-EMF (Brushless DC) Motor Drives

Although the brushless DC motors are equivalent to conventional DC motors with stator and rotor flipped, the construction of BLDC motors is almost similar to permanent magnet synchronous AC motors. The rotor of a BLDC is composed of one or more permanent magnets. The stator windings are similar to those in a poly-phase AC motor. An important difference between the stator of a BLDC motor and a typical brushed DC motor is, since the stator and rotor position are flipped, the commutation has to occur in the stator instead of the rotor in a BLDC motor. The mechanical commutation is replaced by electronic switches in the form of a power

inverter. The stator is connected to the electronic commutation circuit which is composed of an inverter run by a DC voltage input and a controller.

Any brushless DC motor control system requires rotor position information to provide accurate commutation sequence and thus control the gate pulses of the inverter properly. Thus a typical brushless DC motor system, unlike a brushed DC motor system where mechanical commutation occurs in the rotor and hence does not require rotor position information, has position sensors in the form of Hall Effect sensors, absolute position sensors, resolvers etc. Hall Effect sensors are the most commonly used sensors for a typical BLDC drive. A BLDC motor with stator mountable hall sensors for rotor position sensing is shown in Fig. 1-1.

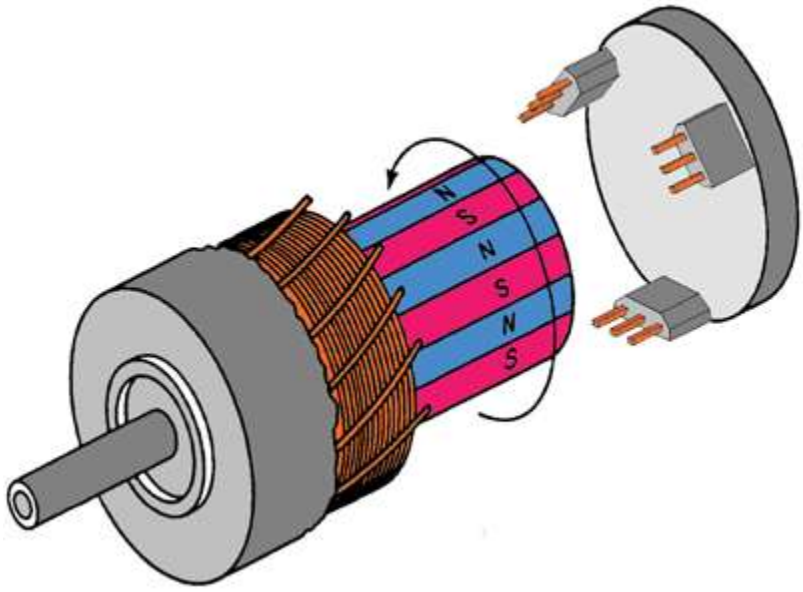

Fig. 1-1. A typical brushless motor with stator mountable Hall effect sensors

Generally, BLDC motors are driven by six-step commutation scheme from a voltage or current source inverter [4]. Commutation occurs in a way that two of the three phases are energized at a time while the other phase is un-energized. Typically the conduction interval between phases is 120°, meaning that the angle gap between each of the phases is 120°. The

inverter gate pulses have to be supplied in a way so that the inverter output terminals provide a sequence that helps 60° commutation for each phase for producing maximum torque which is discussed in Chapter 2. In order to provide accurate commutation timing, rotor position information in necessary which can be provided by Hall sensors in a sensor-ed control or motor parameters in a sensorless control.

Although the BLDC motors do not suffer from wear and tear of the rotor brushes and thus make the control system more robust, the use of position sensors has some drawbacks. Obviously the use of some external components like position sensors increases cost. Although the position sensors are accurate enough for working with speed control mechanisms, for finer controls like position control, they cannot result in very high resolution for accurate position measurements. Reliability issue is one of the biggest concerns now a days in the electric drives industry. In a closed loop system like a BLDC drive, reliability is likely to be affected due to external components like Hall position sensors. These reasons make the sensor-ed control somewhat unpopular and encourage research towards sensorless control scheme.

Many sensorless schemes have been proposed in the last three decades. Those methods can be divided into different categories – back-EMF sensing [5][6][7][8][9], back-EMF integration[10][11], flux linkage based commutation [12][13] and freewheeling diode conduction [14]. Many methods have been proposed to sense the back-EMF of a BLDC motor. In the conventional back-EMF sensing method [8], a virtual neutral point is established with the help of resistors since the actual neutral point of a Y connected squirrel cage motor is not accessible. Theoretically, this virtual neutral point should be at the same potential as the actual neutral point. Assuming so, the voltage difference between the stator terminal and this virtual neutral point

gives the back-EMF of that phase. However, there will be a potential difference between actual and virtual neutral points. Moreover, in an inverter based control system, the neutral point is never standstill. Depending on the gating sequence, it varies from the reference voltage to the maximum DC bus voltage creating a huge common mode voltage. Also, this method creates a lot of noise in the sensed signal and thus requires attenuation and filtering which increases cost and reliability issues and imposes unwanted lag into the system. The most important consequence of this is poor dynamic performance, especially in the low speed range.

In the back-EMF integration method[10][11], the back-EMF of the silent (unexcited) phase is integrated. This has an advantage of reduced switching noise, but the presence of high common mode voltage in the neutral is still a problem. The third harmonic voltage integration[9] [15]has the same limitation. The fundamental idea behind the flux linkage based estimation[13][16] is that the flux linkage of the motor has a direct relationship with the rotor position, and an accurate measurement of flux linkage can lead to the exact rotor position. The flux can be estimated by integrating the voltage in each phase. The poor performance in the low speed is still an issue in this method. Another method is the indirect sensing of zero crossing of back-EMF [14] by detecting the conducting state of the free-wheeling diodes of the inverter. In this method, a tiny current flows through the freewheeling diode in the silent phase. The point at which the current starts flowing is the commutation instant. A serious drawback of this system is the need for several isolated power supplies which increases the complexity. Also, the commutation at the transient state is not good enough. The implementation of this method is complex and also the low speed operation is not quite satisfactory. A back-EMF sensing method is presented in [5] where no neutral point is needed. By appropriately choosing PWM and

sensing strategy, the actual back-EMF can be sensed accurately. In this method, the PWM signals are only applied to the high side switches. One drawback of this system is that it needs a minimum off time for the PWM, which means that 100% duty cycle is not possible. This method provides very accurate results even for low speeds. Later on, an improvement of this method was implemented [7] which made it possible to attain nearly 100 % duty cycle.

In 2004, a speed independent commutation process was presented by Ehsani and Kim [17] which eliminates the speed dependency of the back-EMF waveform, thus making it possible for the control system to attain very accurate results in the low speed range. The concept behind this method is to generate a speed independent commutation function which has no speed term at all in its equation. This method, instead of trying to sense back-EMF of a phase, attempts to find the difference between the back-EMFs of two phases. The ratio of the differences of back-EMF in different phases is speed independent, so the shape becomes exactly the same for all speeds. The commutation instants can be found out from the ratio and thus makes it possible to detect the rotor position. Later on, a similar research [18] was presented based on state observer method[19][20][21]. This method is very accurate and has very good dynamic performance even in the low speed range because of the speed independent commutation function. However, this method suffers from external noise problem.

The objective of this thesis is to present a speed control method for a BLDC drive with and without hall sensors. Experimental results are provided for Hall sensor-ed system and simulation was carried out for a sensorless control method which is based on the research in [17] and [18]. Even though a noise avoidance technique has been presented in [18] based on threshold, an improved noise avoidance technique is presented in this thesis.

The thesis is organized as follows. Chapter 2 describes the fundamentals of Brushless DC motors including its structure and mathematical model. The simulation and experimental results are presented in Chapter 3 for a BLDC drive with Hall sensor mounted. The concept of sensorless control method based on state observer and speed independent commutation function is explained and simulation results are presented in Chapter 4. The control scheme has improved noise sensitivity. Chapter 5 concludes the thesis. The possibilities for future work are also presented.

CHAPTER 2. BRUSHLESS DC MOTOR: CONSTRUCTION AND MATHEMATICAL MODEL

2.1. Construction

Trapezoidal back-EMF (Brushless DC) Motor is basically a permanent magnet synchronous machine which has uniformly distributed winding and a trapezoidal shaped back-EMF. Fig. 1 shows the construction of a 2 pole BLDC motor. This motor consists of a stationary part called stator and a rotating part called rotor. There is a space between stator and rotor called air gap. In a permanent magnet BLDC motor, the rotor carries the magnet. This magnet (rotor) can be inside the stator or outside. Both cases are shown in Fig. 1 [22].

There are two important definitions in most BLDC motors called slot and core. Usually the windings are placed in slots which are kept inside a laminated steel structure called core. A tooth is the section of steel placed in between two slots. Fig. 2-2 shows a BLDC structure with

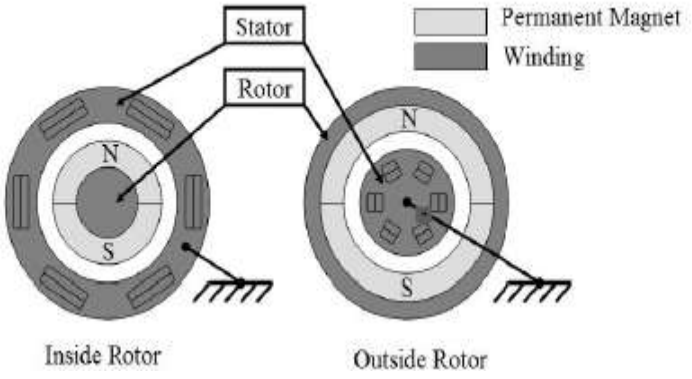

Fig. 2-1. Construction of a 2-pole BLDC motor

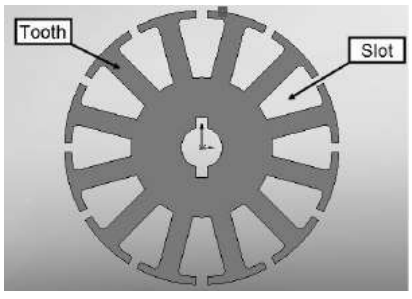

Fig. 2-2. Slot and tooth of a BLDC motor

slots, core and tooth labeled [22]. Most BLDC motors are three phase. A pole is a permanent magnet pole, either north or south. Motors can have any even number of poles.

The mechanical rotation of a motor and the rotation of magnetomotive force (MMF) can be same or different – depending on the number of poles. The relation between these two are defined as Electrical angle = Mechanical angle $\times \frac{P}{2}$, where P = number of poles. Fig. 2-3 illustrates the difference between electrical and mechanical angle.

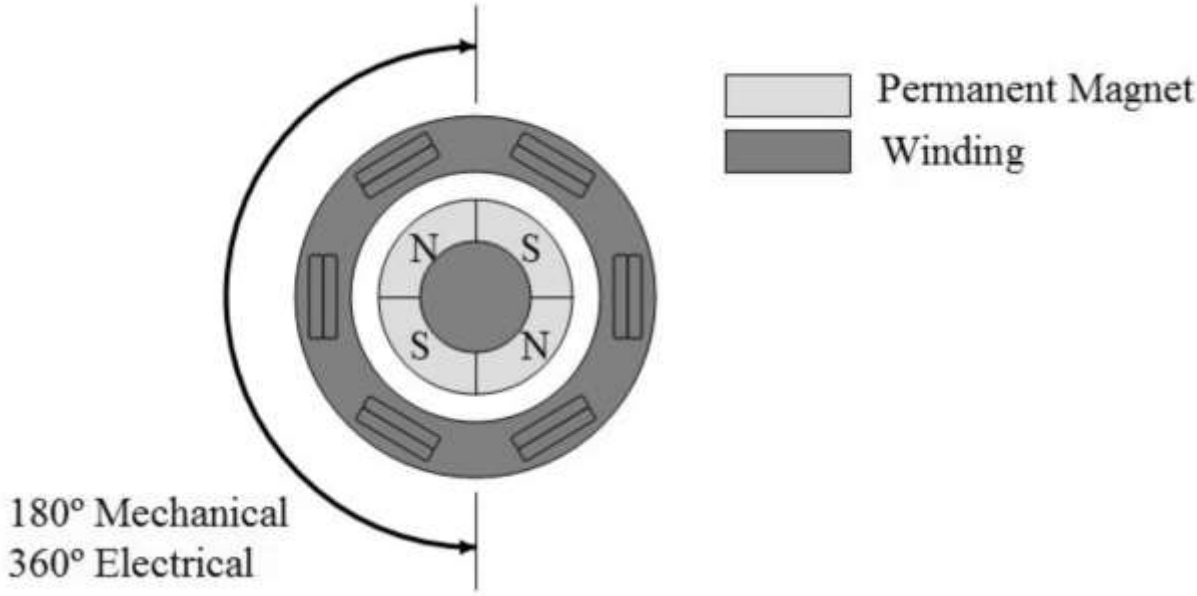

Fig. 2-3. Relation between electrical and mechanical angle of rotor[22]

2.2. Mathematical Model

Permanent magnet motors can be modeled as a speed dependent voltage source with an inductor and a resistor in series. The speed dependent voltage source is popularly known as counter EMF or back EMF (Electromotive Force). This back EMF is generated by moving a current carrying conductor in a changing magnetic field. In case of a typical brushed DC motor,

the back EMF is proportional to speed of the motor. The proportionality constant is called the back EMF constant. The electromechanical model of a brushed DC motor is shown in Fig. 2-4 [22].

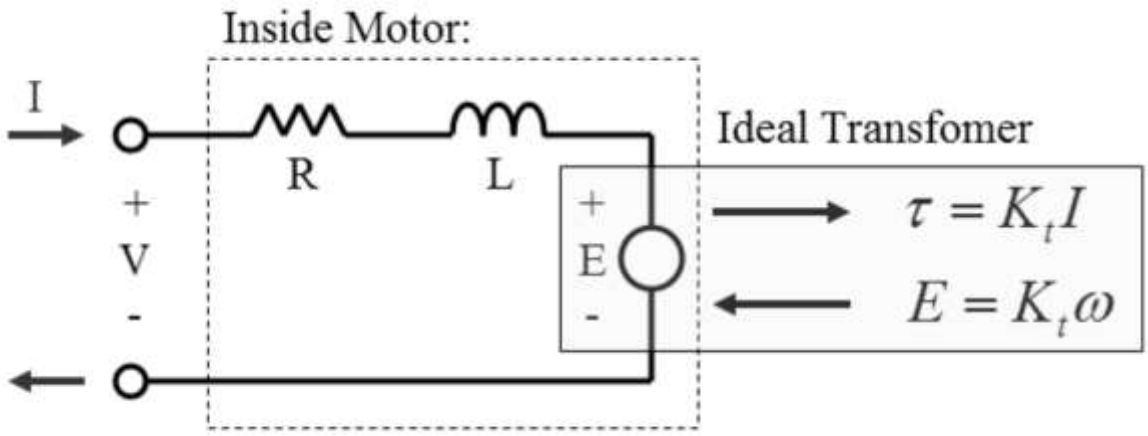

Fig. 2-4. Equivalent circuit of a typical brushed DC motor

The motor constant, referred as K_t or K_v, sets torque per unit current and back EMF per unit speed. Both these units have same SI unit.

In case of a brushless DC motor, the current carrying conductors or winding positions are variable with respect to magnets, unlike the case of a brushed DC motor, where these positions are fixed. This can be modeled by assuming the motor constant K_t (or K_v) to be a periodic function of the electrical angle. This concept is illustrated in Fig. 2-5[22].

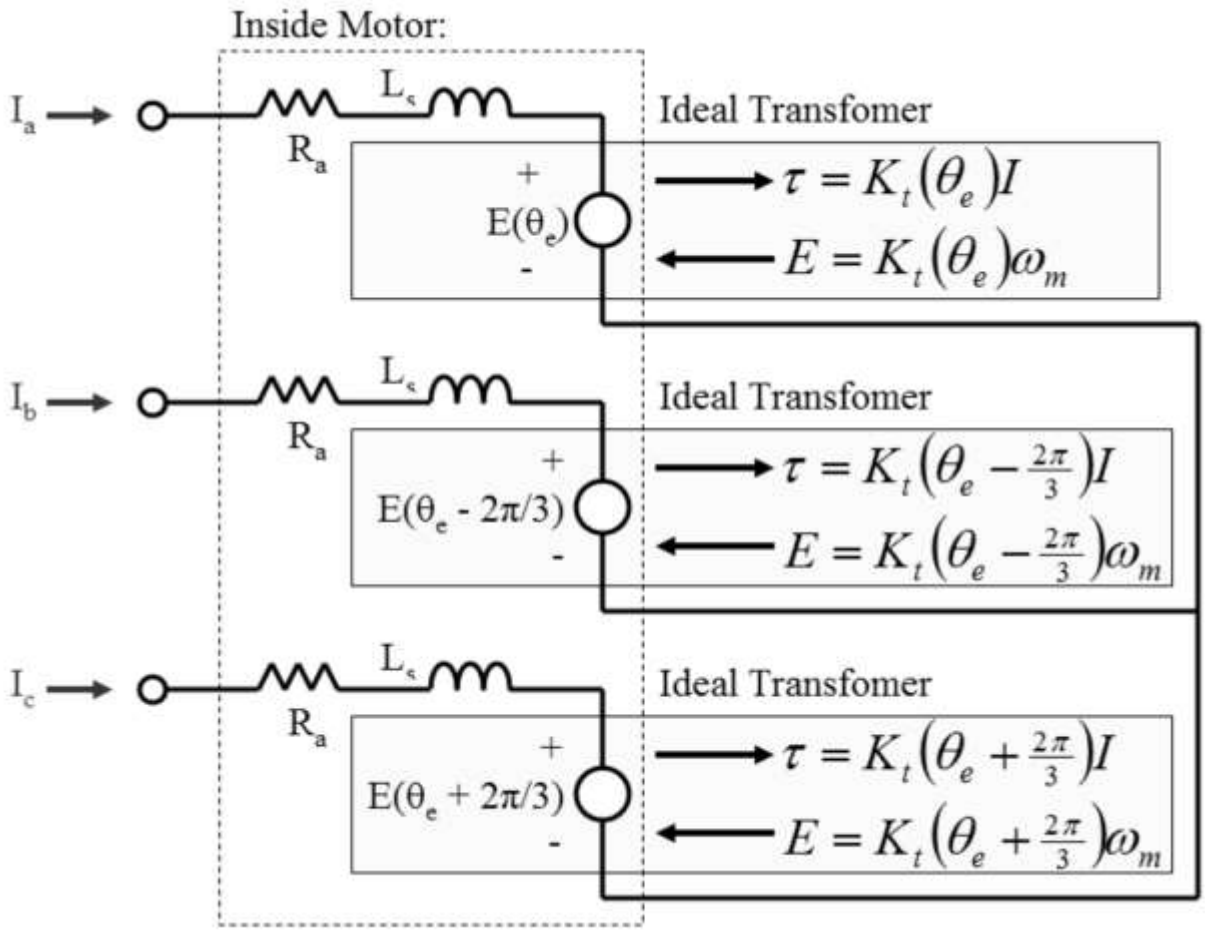

Fig. 2-5. Equivalent circuit of a brushless DC motor

Since the flux distribution of a BLDC motor is trapezoidal, usually the d-q rotor reference frame developed for sinusoidal back EMF motors is not applicable. In this thesis, it is assumed that the induced current in the rotor due to stator harmonic fields are neglected and iron and stray losses are also neglected. A three phase BLDC motor equation can be represented as

$$V_{as} = i_{as}R_s + L_{aa}\frac{\mathbf{d}}{\mathbf{dt}}i_a + M_{ab}\frac{\mathbf{d}}{\mathbf{dt}}i_b + M_{ac}\frac{\mathbf{d}}{\mathbf{dt}}i_c + e_{as} \quad (2.1)$$

$$V_{bs} = i_{bs}R_s + L_{bb}\frac{d}{dt}i_b + M_{ba}\frac{d}{dt}ia + M_{bc}\frac{d}{dt}i_c + e_{bs} \quad (2.2)$$

$$V_{cs} = i_{cs}R_s + L_{cc}\frac{d}{dt}i_c + M_{ca}\frac{d}{dt}i_a + M_{cb}\frac{d}{dt}i_b + e_{cs} \quad (2.3)$$

The coupled circuit equations of the stator windings are as follows[4] [23]:

$$\begin{bmatrix} v_{as} \\ v_{bs} \\ v_{cs} \end{bmatrix} = \begin{bmatrix} R_s & 0 & 0 \\ 0 & R_s & 0 \\ 0 & 0 & R_s \end{bmatrix} \begin{bmatrix} i_{as} \\ i_{bs} \\ i_{cs} \end{bmatrix} + p \begin{bmatrix} L_{aa} & L_{ab} & L_{ac} \\ L_{ba} & L_{bb} & L_{bc} \\ L_{ca} & L_{cb} & L_{cc} \end{bmatrix} \begin{bmatrix} i_a \\ i_b \\ i_c \end{bmatrix} + \begin{bmatrix} e_{as} \\ e_{bs} \\ e_{cs} \end{bmatrix} \quad (2.4)$$

Where,

R_s = Stator resistance per phase, assuming equal resistances in each phase

I_{as}, I_{bs}, I_{cs} = stator currents in each phase

L_{aa}, L_{bb}, L_{cc} = stator self-inductances in each phase

L_{ab}, L_{ba}, L_{bc}, L_{cb}, L_{ca}, L_{ac} = mutual inductance of the stator phases and the rotor magnet

e_{as}, e_{bs},e_{cs} = induced EMF or back EMF in each phase.

The shape of the back EMFs are all assumed to be trapezoidal, with the peak value E_p as $E_p = \lambda_p\omega_m$, where λ_p = flux linkage constant and ω_m = rotor electrical speed in rad/s.

In an ideal situation, it can be assumed that rotor reluctances are constant with respect to rotor electrical angle. Also, if the three phases are symmetric, then the self-inductances in all phases can be assumed equal and the mutual inductances between phases are equal to one another. So if we call the mutual inductance to be M and self-inductance to be L, then effectively, $L_{ab} = L_{bc} = L_{ca} = L_{ba} = L_{cb} = L_{ac} = M$ and $L_{aa} = L_{bb} = L_{cc} = L$, and equation (2.4) becomes

$$V_{as} = i_{as}R_s + L\frac{d}{dt}i_a + M\frac{d}{dt}i_b + M\frac{\mathbf{d}}{\mathbf{dt}}i_c + e_{as} \quad (2.5)$$

$$V_{bs} = i_{bs}R_s + L\frac{\mathbf{d}}{\mathbf{dt}}i_b + M\frac{d}{dt}i_a + M\frac{d}{dt}i_c + e_{bs} \quad (2.6)$$

$$V_{cs} = i_{cs}Rs + L\frac{d}{dt}i_c + M\frac{\mathbf{d}}{\mathbf{dt}}i_a + M\frac{\mathbf{d}}{\mathbf{dt}}i_b + e_{cs} \quad (2.7)$$

The equation can be written in a matrix form as,

$$\begin{bmatrix} v_{as} \\ v_{bs} \\ v_{cs} \end{bmatrix} = R_s \begin{bmatrix} 1 & 0 & 0 \\ 0 & 1 & 0 \\ 0 & 0 & 1 \end{bmatrix} \begin{bmatrix} i_{as} \\ i_{bs} \\ i_{cs} \end{bmatrix} + \begin{bmatrix} L & M & M \\ M & L & M \\ M & M & L \end{bmatrix} p \begin{bmatrix} i_a \\ i_b \\ i_c \end{bmatrix} + \begin{bmatrix} e_{as} \\ e_{bs} \\ e_{cs} \end{bmatrix} \quad (2.8)$$

Assuming balanced three phase currents, the equation (2.8) can be further simplified as [4],

$$\begin{bmatrix} v_{as} \\ v_{bs} \\ v_{cs} \end{bmatrix} = \begin{bmatrix} R_s & 0 & 0 \\ 0 & R_s & 0 \\ 0 & 0 & R_s \end{bmatrix} \begin{bmatrix} i_{as} \\ i_{bs} \\ i_{cs} \end{bmatrix} + \begin{bmatrix} (L-M) & 0 & 0 \\ 0 & (L-M) & 0 \\ 0 & 0 & (L-M) \end{bmatrix} p \begin{bmatrix} i_a \\ i_b \\ i_c \end{bmatrix} + \begin{bmatrix} e_{as} \\ e_{bs} \\ e_{cs} \end{bmatrix} \quad (2.9)$$

which is identical to the equation of a brushed DC motor. This is part of the reason for which this machine is called brushless DC motor.

Neglecting mutual inductances,

$$V_{as} = i_{as}R_s + L\frac{d}{dt}i_a + e_a \quad (2.10)$$

$$V_{bs} = i_{bs}R_s + L\frac{d}{dt}i_b + e_{bs} \quad (2.11)$$

$$V_{cs} = i_{cs}Rs + L\frac{d}{dt}i_c + e_{cs} \quad (2.12)$$

2.3. Trapezoidal vs. Sinusoidal Back EMF

Counter EMF or Back EMF is the voltage that is produced at the terminals of a motor as a function of rotor position with no load. Back EMF opposes the main voltage supplied to the windings according to Lenz's Law. Even though the shape of the motor back-EMF doesn't change with speed, the amplitude of it is proportional to the rotor angular velocity which can be written as,

$e = \frac{d}{dt}\lambda p$, where λp, rotor flux linkage is a function of rotor angular position. Since the back EMF is the rate of change of rotor flux linkage in the winding, it can be safely stated that the amplitude of the back EMF is dependent on or a function of angular velocity and the shape of back EMF is a function of angular position. Back EMF shapes can be of two types – sinusoidal and trapezoidal. Fig. 2-6 shows [22] normalized sinusoidal and trapezoidal waveforms in ideal conditions.

There are several possible reasons that a motor can have trapezoidal back-EMF. Some of them are

- Concentrated windings

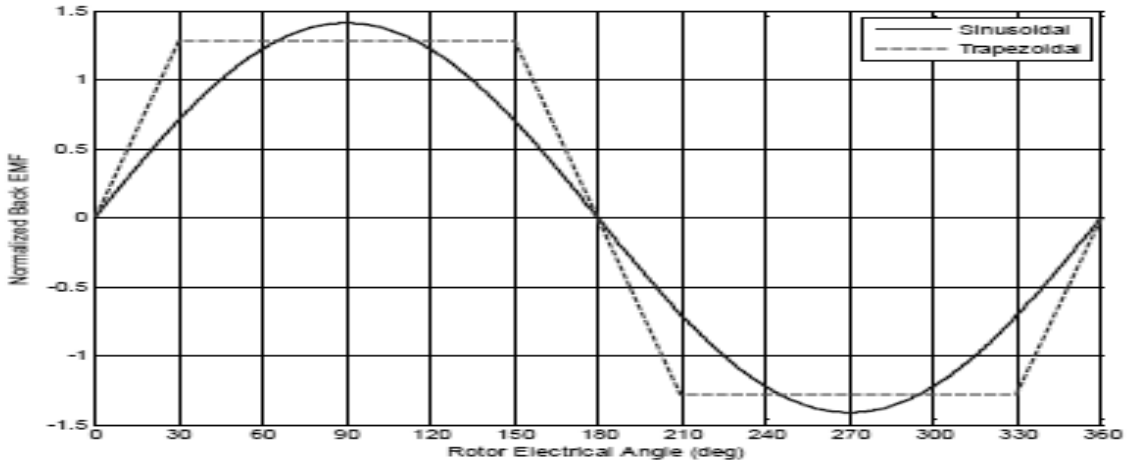

Fig. 2-6. Sinusoidal vs. trapezoidal waveforms

- No stator or magnet skew
- Discrete magnet poles with uniform magnetization

It is important to understand that the stator core saturation is not the reason for the flat top portion of back-EMF of BLDC motors.

On the other hand, the reasons that a motor can have sinusoidal back-EMF are

- Sinusoidally distributed windings
- Sinusoidal magnetization
- Stator without any steel lamination etc.

2.4. Sine Wave Drive vs. Trapezoidal Wave Drive

Though a motor with any back-EMF shape (trapezoidal or sinusoidal) can be driven by either square wave or sine wave drive, motors with trapezoidal back EMF are driven with six-step square wave commutation which is considered to be square wave drive. Motors with sinusoidal back EMF has sinusoidal commutation drive scheme or AC drive.

Square wave drive or six-step commutation is the simplest drive scheme [4][23]. The main concept of this scheme is, at any given instant, one of the three phases of the motor will be sourcing current, one will be sinking current and the rest one will do nothing. Thus, at that instant, one of the inverter pole pairs switches will be turned on and the other will be off. This leaves six possible states, which are shown in Table 1[22]. Each state is active for 60° electrical. It is possible to figure out the active state and thus rotor position by using Hall effect sensors which eventually can be used for driving the controller.

Table 2-1. Possible states for different Hall signal combination

Electrical Angle	Hall Effect State	Phase A	Phase B	Phase C
0°-60°	{0,0,1}	+	-	Off
60°-120°	{0,1,1}	+	Off	-
120°-180°	{0,1,0}	Off	+	-
180°-240°	{1,1,0}	-	+	Off
240°-300°	{1,0,0}	-	Off	+
300°-360°	{1.0,1}	Off	-	+

The purpose of sinusoidal commutation scheme is to provide sinusoidal current in three phases of the motor so that sinusoidal back-EMF can be generated. In order to generate sinusoidal current and to control the motor, high frequency PWM (Pulse Width Modulation) is used in the inverter. The gate pulses of the inverter is given in a way so that the inverter output can be a sinusoidally varying square wave voltage, which is applied to the motor phases and motor phase inductances make filters the square wave voltage PWM intro a sinusoidal current.

The following figure (Fig. 2-7) illustrates the difference between sinusoidal and six step commutation current waveforms with a normalized RMS value of 1.

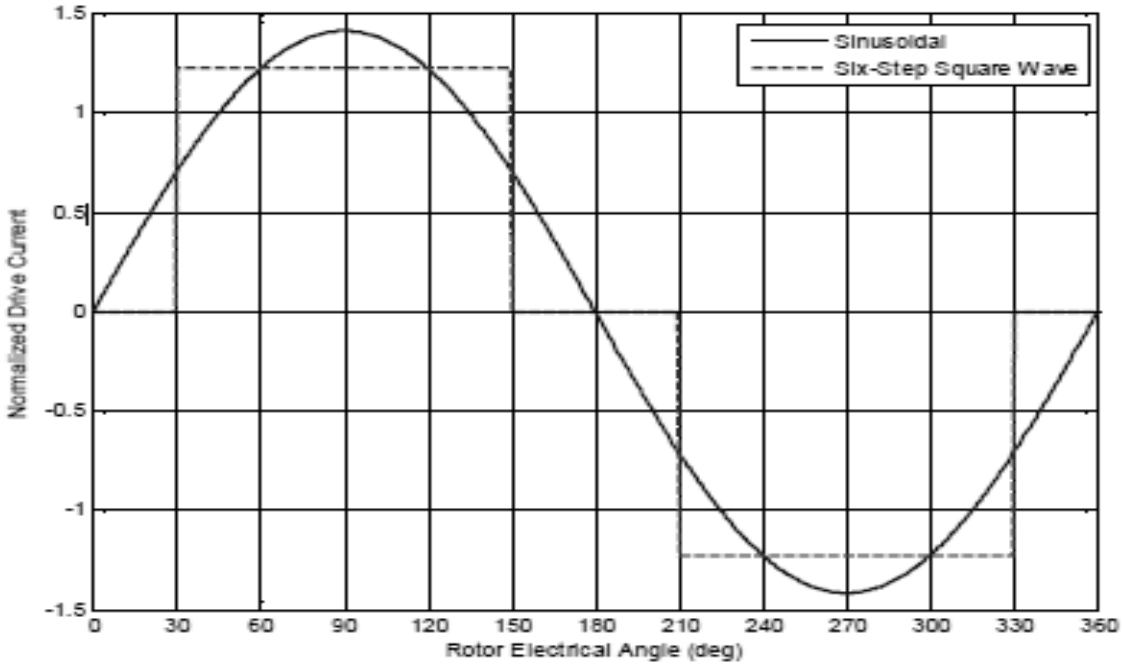

Fig. 2-7. Difference between sinusoidal and six step current

2.5. Torque of BLDC Motor

The electromagnetic torque of a BLDC motor is given by

$$T_e = \left[e_{as}i_{as} + e_{bs}i_{bs} + e_{cs}i_{cs}\right]\frac{1}{\omega_m} \tag{2.13}$$

The instantaneous induced EMF can be written as [4][23]

$$e_{as} = f_{as}(\theta)\lambda_p\omega_m$$

$$e_{bs} = f_{bs}(\theta)\lambda_p\omega_m$$

$$e_{cs} = f_{cs}(\theta)\lambda_p\omega_m \tag{2.14}$$

Where f_{as}, f_{bs}, f_{cs} functions determine the shape of back EMF. This function has a maximum magnitude of ±1.

Rearranging (13) and (14), the electromagnetic torque can be written as

$$T_e = \lambda_p [f_{as}(\theta)\, i_{as} + f_{bs}(\theta)\, i_{bs} + f_{cs}(\theta)\, i_{cs}] \qquad (2.15)$$

Under steady state, one phase of a BLDC motor is unexcited while current flows through the other two phases. Since the back-EMF of a BLDC is trapezoidal, if the phases can be excited during the flat portion of the back-emf, according to (2.13), torque can be maintained constant and thus a stable control can be attained. Fig. 2-8 shows the trapezoidal back-EMFs and phase currents of 3-phase BLDC motor.

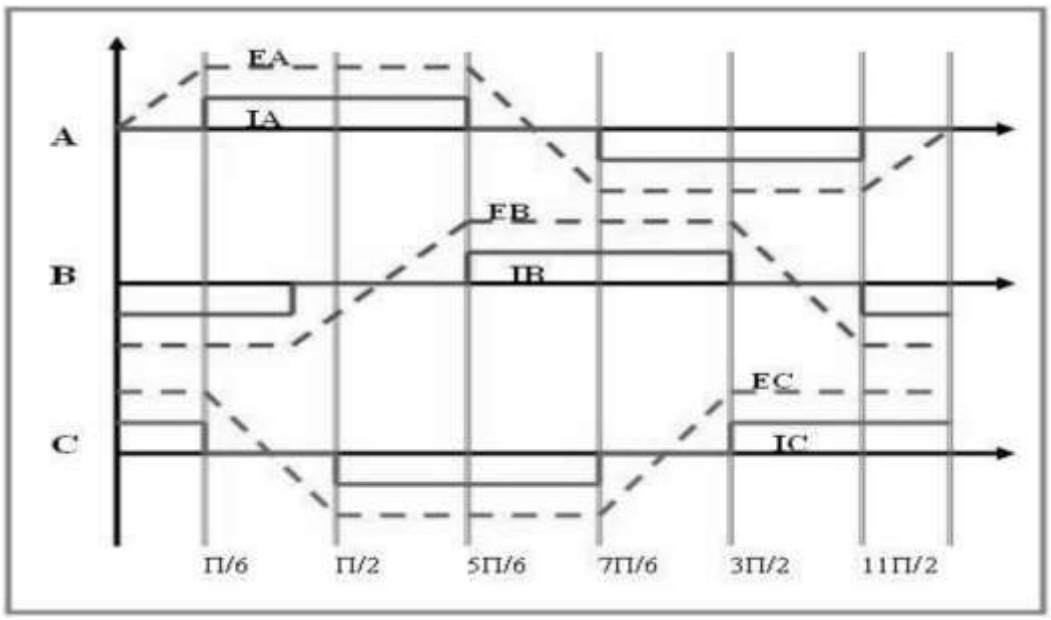

Fig. 2-8. Phase currents and back EMFs of a three phase BLDC motor

CHAPTER 3. BLDC MOTOR DRIVE: HALL SENSOR BASED CONTROL

3.1. BLDC Drive Scheme

Since the trapezoidal back EMFs have constant magnitude for electrical 120° both in positive and negative half cycles **(**Fig. 3-1) [4], the power and torque output can be made uniform by exciting rotor phases with electrically 120° wide current. Since the change in current cannot be instantaneous, current cannot rise and fall abruptly, so there are power pulsations during the turn on and turn off times of currents.

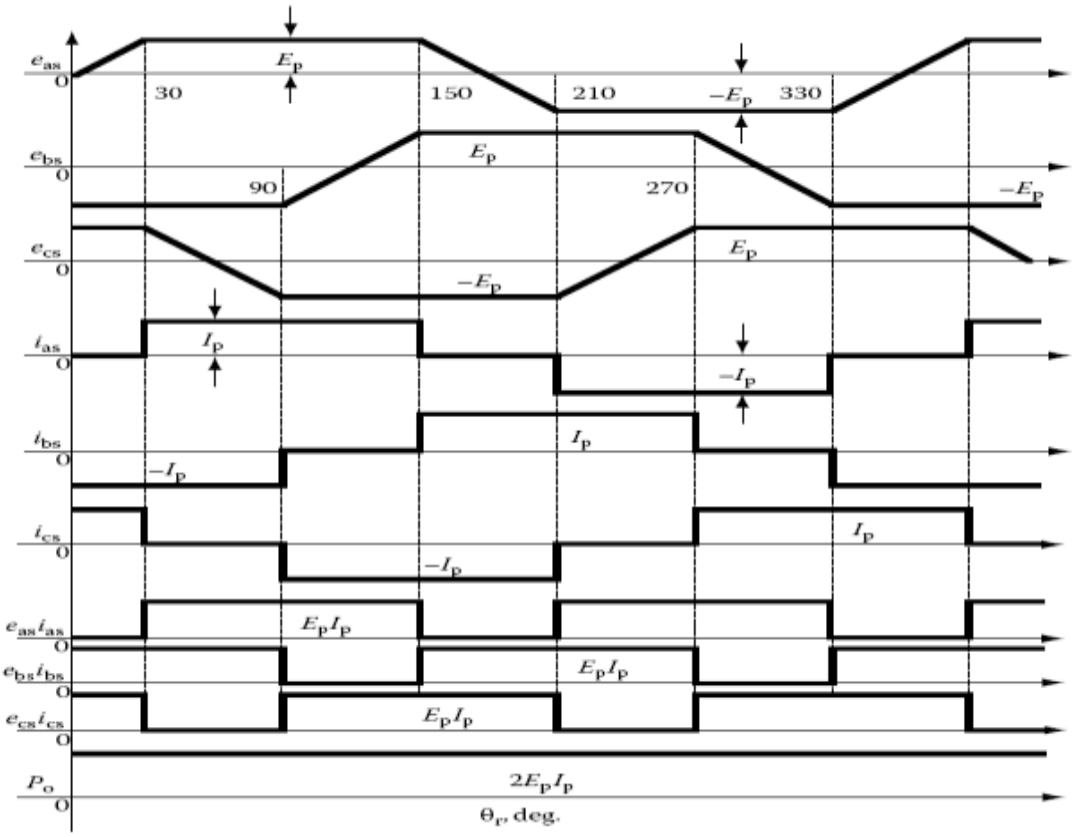

Fig. 3-1. All phase currents and back EMFs of a three phase BLDC motor

In order to have currents aligned with back EMF to get constant torque and power, rotor position information is mandatory. Only two motor phases conduct current at a time for a full wave inverter operation. For the figure above (Fig. 3-1), it evident that one phase is conducting a positive current, one phase is conducting negative current with respect to the previous, and the last phase is non-conducting at a certain time. Referring to (2.15) in the previous chapter, the electromagnetic torque that is expected to be produced is

$$T_e^* = \lambda_p [1 \times I_{as}^* + (-1) \times (-I_{bs}^*) + 0 \times I_{cs}^*] \quad (3.1)$$

For a balanced system, we assume $I_{as}^* = I_{bs}^* = I_{cs}^* = I_p^*$. So the equation of T_e^* becomes

$$T_e^* = 2 \times \lambda_p \times I_p^* \quad (3.2)$$

Once the reference torque is found, the stator command current can be calculated as

$$I_p* = \frac{T_e}{2\lambda_p} \quad (3.3)$$

3.2. Control Schemes

Typically, three different control schemes are applicable in case of BLDC motors – hysteresis band control, PWM control and variable DC link voltage control [23][24]. Each control method has its own advantage and drawbacks. Use of these methods depends on the specific application and parts of the control system.

3.2.1. Hysteresis Band Control

This control scheme is one of the simplest and most common closed loop control methods. In this hysteresis control method, the value of the controlled variable is forced to stay

within certain limits which is called hysteresis band, around a specific commanded value. If hysteresis band is to be applied to motor speed, for example, then once the motor will reach and exceed the speed, it will stop rotating, then once the speed goes below at that or another certain level, it will start again. Obviously, this is not a very good method to control a motor speed, so it is understandable that hysteresis control cannot be applied to every application. The drawback of this method is high and uncontrolled switching frequency in a very narrow range or hysteresis band is used and ripples become large if the band is wider [24]. The switching frequency is unknown and depends on the band width. This unknown switching frequency makes the control difficult to filter electromagnetic and audible noises. Typical phase current waveforms of a BLDC hysteresis torque control is shown below[24].

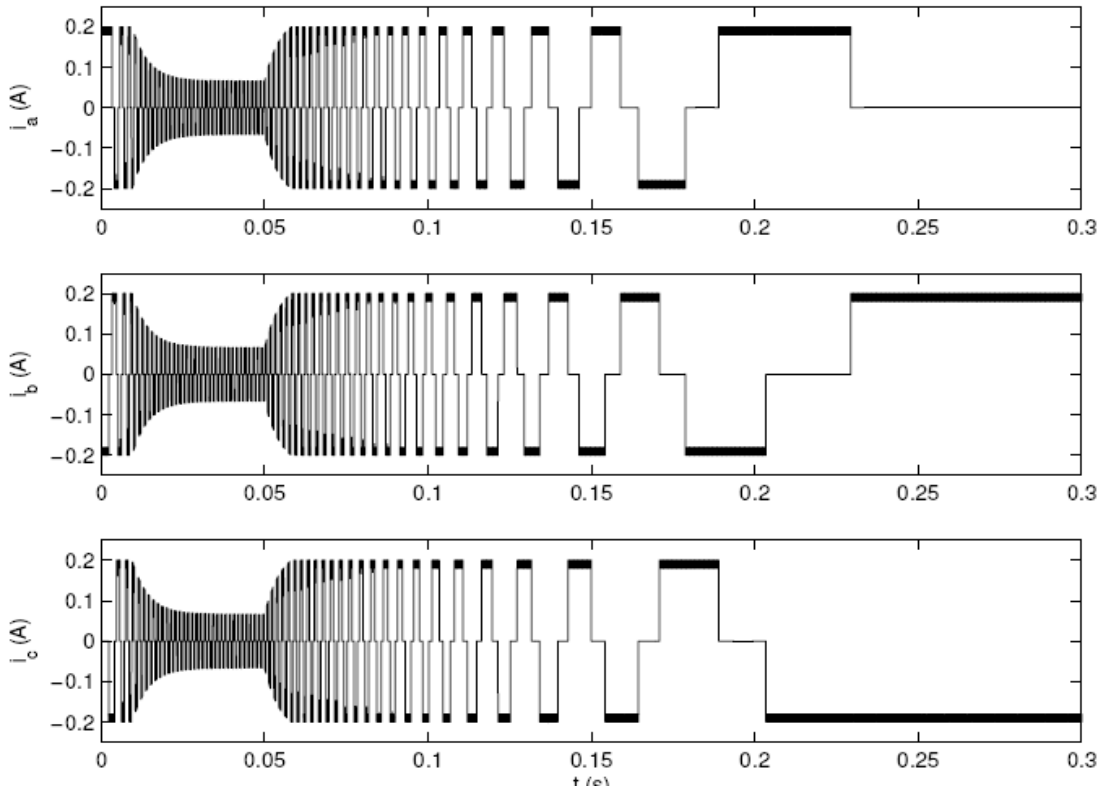

Fig. 3-2. Typical phase current waveforms in hysteresis torque control method

3.2.2. PWM Control

In this control method, a chopper or an inverter is used to control the motor and the gate pulses are controlled using Pulse Width Modulation. Typically the chopping frequency is fixed but the duty cycle is variable. Since the frequency is fixed, switching noises can be filtered easily compared to hysteresis band control. In this control method, switches are turned on and off frequently and their on time and off time are controlled according to an error signal. Thus, if the error is getting more, then the corresponding gates are turned on for more time. The current and voltage are sampled with a high frequency and thus typical BLDC phase currents are similar to (3.3) [24]

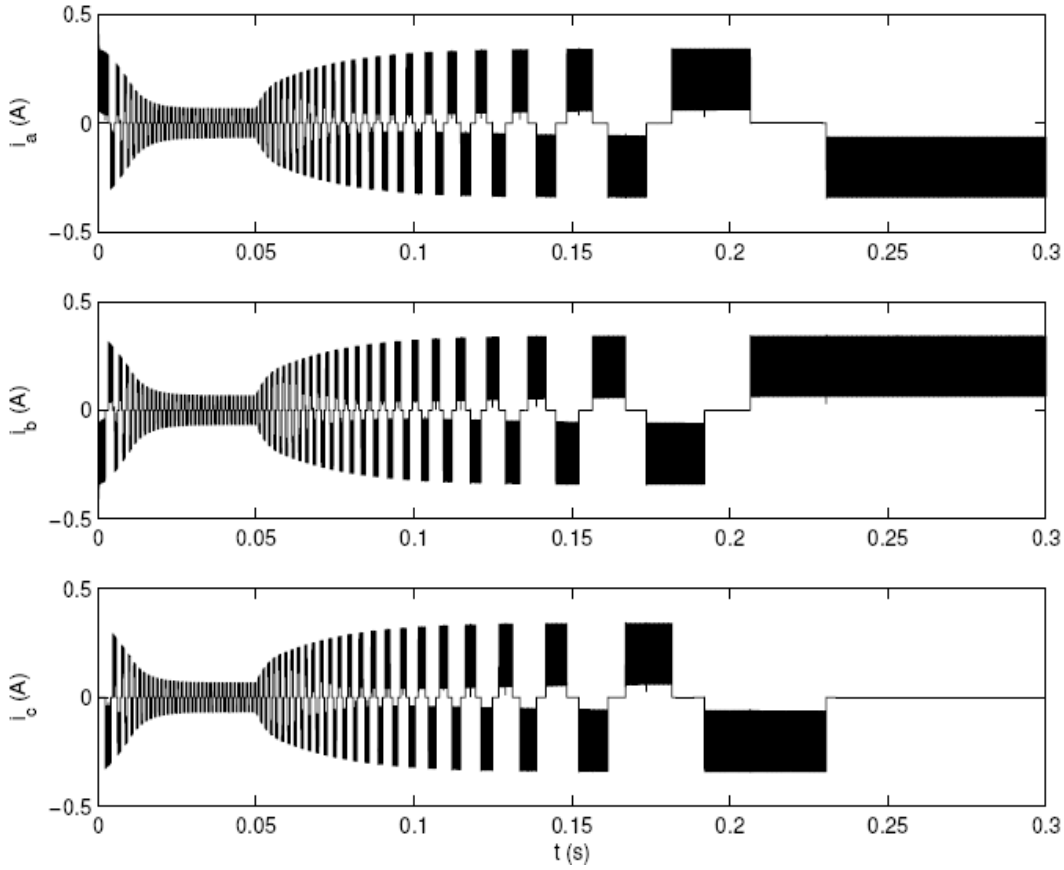

Fig. 3-3. Typical phase current waveforms in PWM control method

3.2.3. Variable DC Link Voltage Control

In this method, the DC link voltage coming from the output of a three phase rectifier is controlled. This method has some advantages and disadvantages over the previous two methods. The system can be cheaper than the PWM control method, but at the same time losses can be high at low voltage and high current [24]. However, this method can provide best solution in high speeds in terms of less switching loss because at high speeds, those losses are significant in PWM control method. Typical phase currents waveforms in this method are given below in Fig. 3-4 [24]

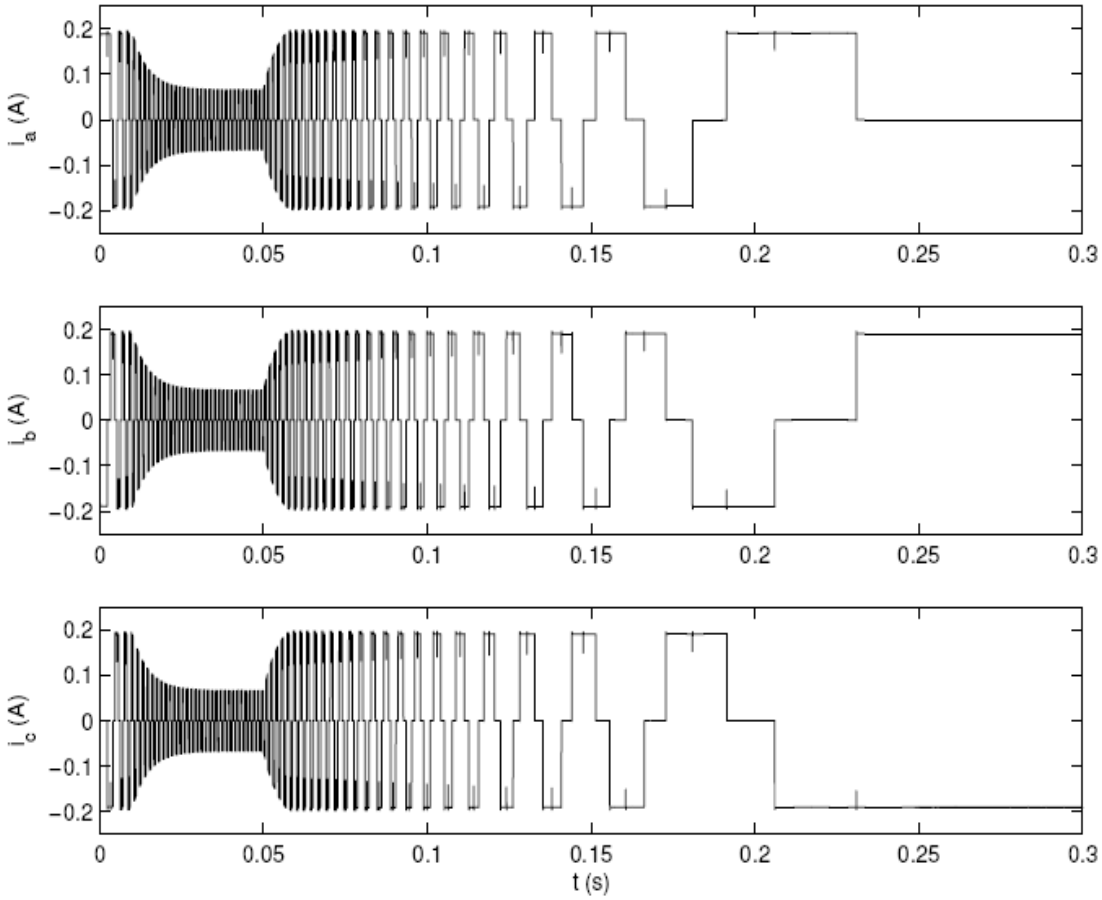

Fig. 3-4. Typical phase current waveforms in variable DC link voltage control method

In this thesis, PWM control has been used in the inverter for speed control (outer loop) of BLDC motor and hysteresis control has been used for current control (inner loop). In case of a hysteresis current control, the voltage source is controlled by a fast-acting current source [4]. The actual current is controlled within a narrow band from its desired value in this hysteresis control. The reference current and the actual current are shown is Fig. 3-5 with the hysteresis windows and gate signals [4][23]

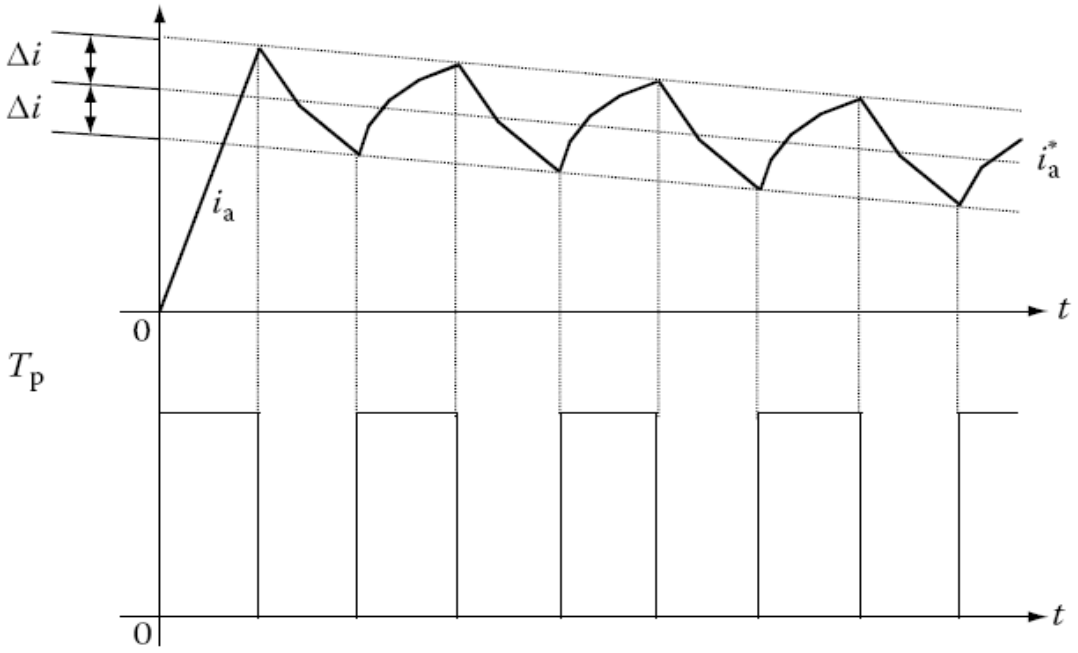

Fig. 3-5. Hysteresis band control

The applied voltage to the load is determined by the following logic:

$i_a \leq i_a^* - \Delta i$, set $v_0 = V_s$

$i_a \leq i_a^* + \Delta i$, set $v_0 = 0$

This current control method is simple and easy to implement, however, this has a drawback of variable and unknown switching frequency.

3.3. Hall Sensor Based BLDC Speed Control

Fig. 3-6 shows [4][23] the basic block diagram for a typical BLDC motor control system. Three hall sensors are used which are placed 120 physical degrees apart from each other.

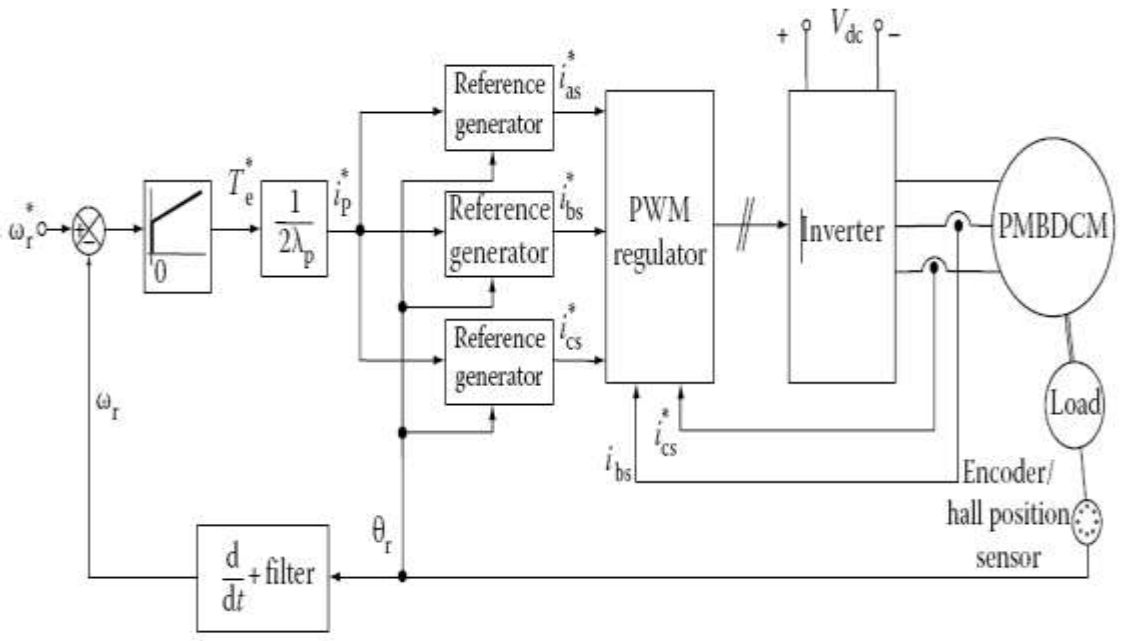

Fig. 3-6. A complete BLDC speed control system with hall sensor for position information

As shown in Fig. 3-6, hall position sensors provide the information of rotor position from which rotor speed can be calculated. The inner loop enforces current command and outer loop enforces speed command. Rotor speed is compared with the reference or commanded speed to produce some error speed which is initially equal to reference speed and equals zero at ideal steady state. The error is processed with a PI controller with appropriate proportional and integral constants to produce the reference torque for the drive. The commanded current is found from the reference torque from equation (3.3). Rotor positions extracted from Hall sensors are translated to three different states (1, 0, -1) depending on the rotor instantaneous positions. These

states have the exact match with the states of the respective back EMFs, and hence multiplied with the commanded current to produce reference current vectors which are compared to the actual currents respectively (hysteresis control). The error signal produced from this comparison is used as a reference for a PWM generator block which provides 6 gate pulses for the three phase inverter.

3.4. Design of the Drive System

3.4.1. Modeling of the Motor with Converter

For modeling the BLDC motor and the inverter, we assume that the conduction voltage drop is zero and there is no switching time loss. In order to model a conducting phase of the motor, the system equation can be written as

$$R_s + L_s \frac{di_s}{dt} + e_{as} = V_s \tag{3.4}$$

Where,

R_s = Stator resistance per phase

L_s = self-inductance of a phase

i_s = phase current

e_{as} = phase back EMF

V_s = DC link voltage

The back EMF is given by [4]

$$e_{as} = K_b f_{as}(\theta) \omega_m \tag{3.5}$$

where f_{as} is a function which has identical shape with the back EMF and has value changing with respect to rotor position.

f_{as} is given by [4]

$$
\begin{aligned}
f_{as}(\theta) &= (\theta)\,\frac{6}{\pi}, && 0 < \theta < \frac{\pi}{6} \\
&= 1, && \frac{\pi}{6} < \theta < \frac{5\pi}{6} \\
&= (\pi - \theta)\,\frac{6}{\pi}, && \frac{5\pi}{6} < \theta < \frac{7\pi}{6} \\
&= -1, && \frac{7\pi}{6} < \theta < \frac{11\pi}{6} \\
&= (\theta - 2\pi)\,\frac{6}{\pi}, && \frac{11\pi}{6} < \theta < \frac{2\pi}{6}
\end{aligned}
\tag{3.6}
$$

The electromechanical equation with load is given by,

$$J\frac{d\omega_m}{dt} + B\omega_m = T_e - T_l \tag{3.7}$$

where

J is the moment of inertia

B is the friction coefficient

T_l is the load torque

T_e is the electromagnetic torque given by [4]

$$T_e = K_t\,[f_{as}(\theta)\, i_{as} + f_{bs}(\theta)\, i_{bs} + f_{cs}(\theta)\, i_{cs}] \tag{3.8}$$

where K_t is the constant of torque and is equal to $\lambda_p(\frac{p}{2})$, where p is number of motor pole.

3.4.2. Modeling the Speed Controller

For outer loop (speed loop), a proportional integral (PI) control is used. The speed controller is modeled as

$$G(s) = Kps + \frac{Ki_s}{s} \tag{3.9}$$

where s is a Laplace operator.

This equation is the key equation for deriving current and torque reference. Fig shows the state diagram for the speed controller [4]. The limiter at the end of the figure is used to restrict the reference torque generated within a permissible limit in order to avoid uncontrolled situation.

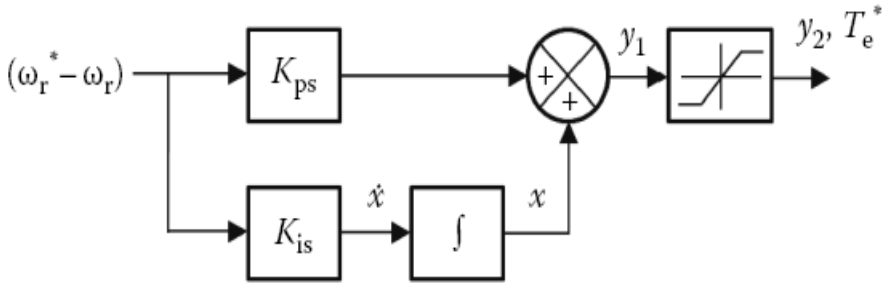

Fig. 3-7. State diagram for the speed controller

From Fig. 3-7, the equation of the reference torque is found as [4]

$$\dot{x} = K_{is}(\omega_r^* - \omega_r) \tag{3.10}$$

$$y1 = \{Kps(\omega r^* - \omega r) + Kis\} \tag{3.11}$$

$$Te^* = y1; \quad Tem \le y1 \le Tem \tag{3.12}$$

where T_{em} = maximum permissible reference torque.

3.4.3. Modeling the Steering Circuit

The steering circuit defines the operational quadrant relationship between speed, torque and phase sequence. The current magnitude command and the polrarity signals of the rotor speed and torque reference are the three inputs for the steering circuit. phase current commands are The determined depending on the quadrant of operation and rotor position. In this thesis, we are one direction only about rotation in ednconcer, so only quadrant1 and4 as are considered described by the equations of Fig. ref] 16. rishnank]:

Quadrant I	**Quadrant I**
$f_{as}(\theta) \geq 1,\ i_{as}^{*} = \lvert i^{*} \rvert$	$f_{as}(\theta) \leq -1,\ i_{as}^{*} = \lvert i^{*} \rvert$
$f_{bs}(\theta) \geq 1,\ i_{bs}^{*} = \lvert i^{*} \rvert$	$f_{bs}(\theta) \leq -1,\ i_{bs}^{*} = \lvert i^{*} \rvert$
$f_{cs}(\theta) \geq 1,\ i_{cs}^{*} = \lvert i^{*} \rvert$	$f_{cs}(\theta) \leq -1,\ i_{cs}^{*} = \lvert i^{*} \rvert$

Fig. 3-8. Quadrant operation of a BLDC motor

3.4.4. Modeling the Current Loop

The current controller has a hysteresis current controller as described previously instead of a PI controller used in the speed loop. The current reference magnitude is determined from the reference torque generated (3.3). This reference magnitude is multiplied by the transmitted Hall signal as described in section 3.3 and compared with actual current to get the error current i_{er}. The output of the current controller is limited to its maximum possible value i_{max}. The output of the hysteresis band controller determines the switching signals for the inverter and the duty cycle of the switching is found by

$$d = \frac{i_{er}}{i_{max}}, \; i_{er} > 0$$

$$= 0, \; ier < 0 \qquad (3.14)$$

time of the switch is given by-The on

where

Tc = PWM cycle period

f_c = PWM frequency

3.4.5. Simulation Results

A BLDC speed control system described in section 3.3 (Fig. 3-6) is simulated in Simulink. A three phase inverter is to generate voltage waves required to generate trapezoidal back EMF. A brushless DC motor is simulated by creating an electrical and mechanical model (Fig. 3-9 and Fig. 3-10)

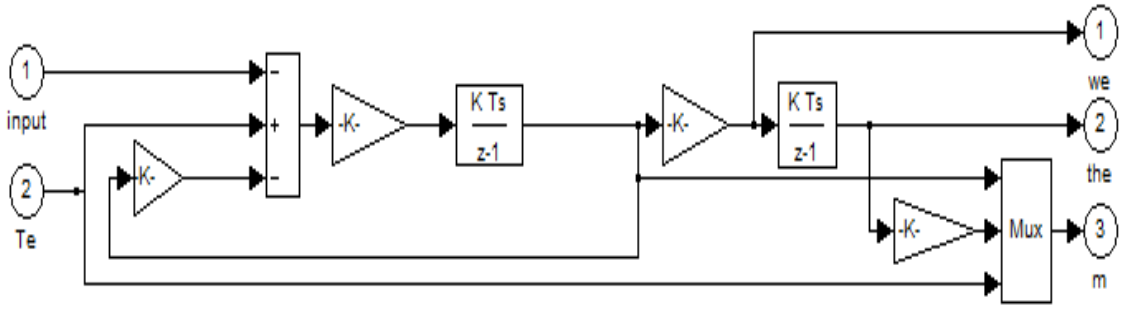

Fig. 3-9. BLDC motor model (electrical)

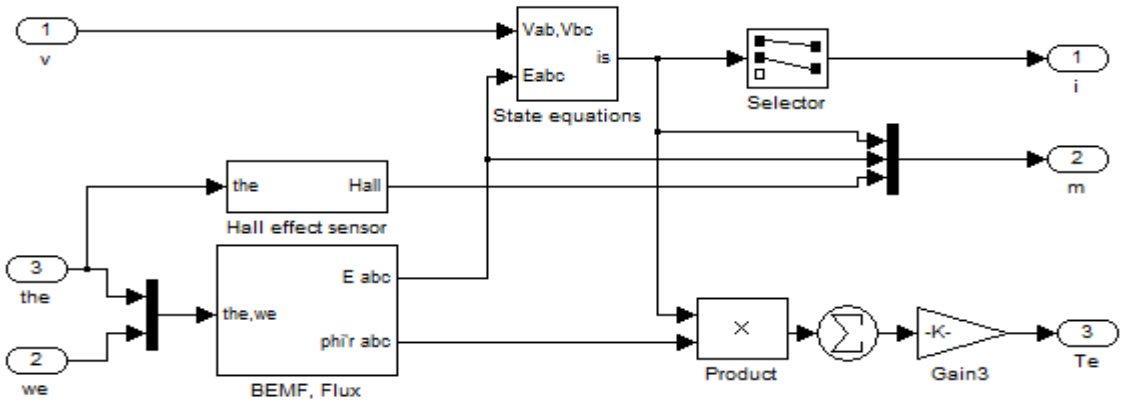

Fig. 3-10. BLDC motor model (mechanical)

The system has been simulated for a 25V, 4-pole, 3 phase BLDC motor for different speed ranges and loads. A voltages source inverter was used to run the motor with its gate controlled by hysteresis current controller. Fig shows key simulation waveforms, measured for a step speed command of 0 to 1500 RPM and then back to 50 RPM.

Motor parameters:

Stator phase resistance: 0.2 Ω

Stator phase inductance: 0.0085 H

Flux linkage: 0.14324 Vs

Voltage constant: 5 v/1000 RPM

Torque constant: 0.57296 Nm / A peak

Inertia: 0.0009 kg*m^2

Friction constant: 0.0005 N*m*s

No of poles: 4

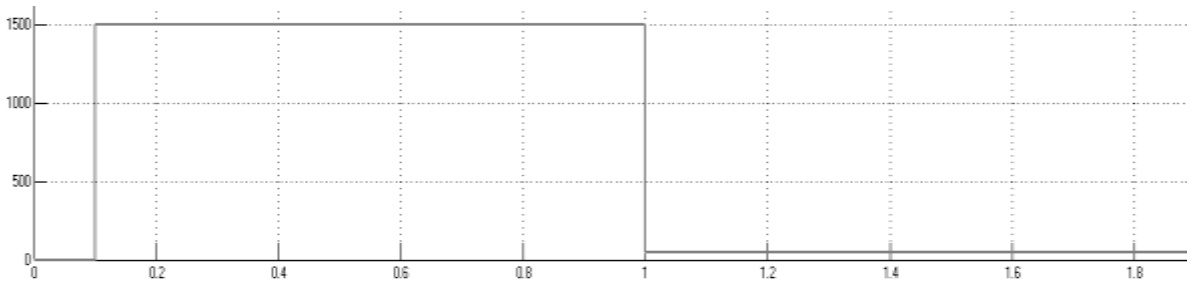

Fig. 3-11. Speed command (RPM) from 0 to 1500 RPM and then 50 RPM

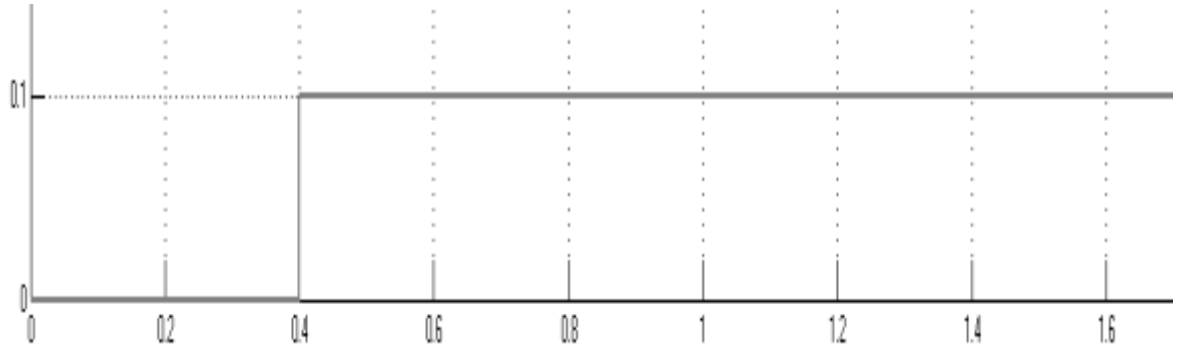

Fig. 3-12. Load torque (Nm)

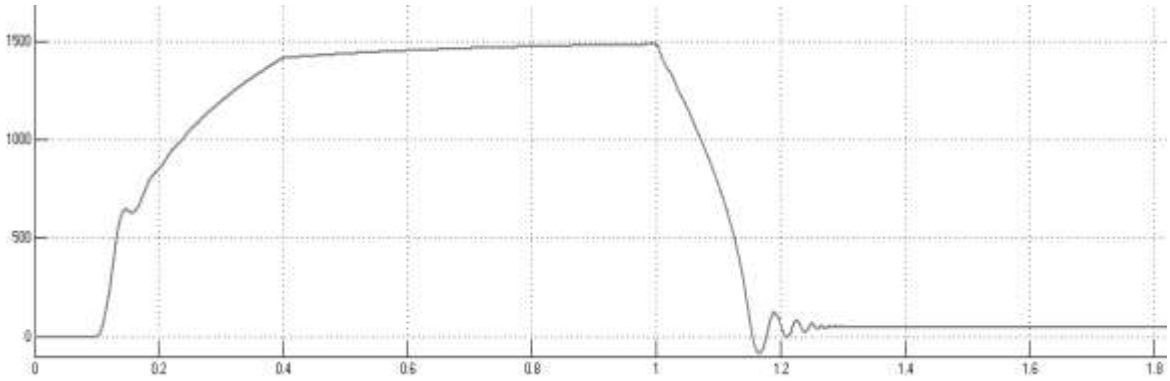

Fig. 3-13. Speed response (RPM)

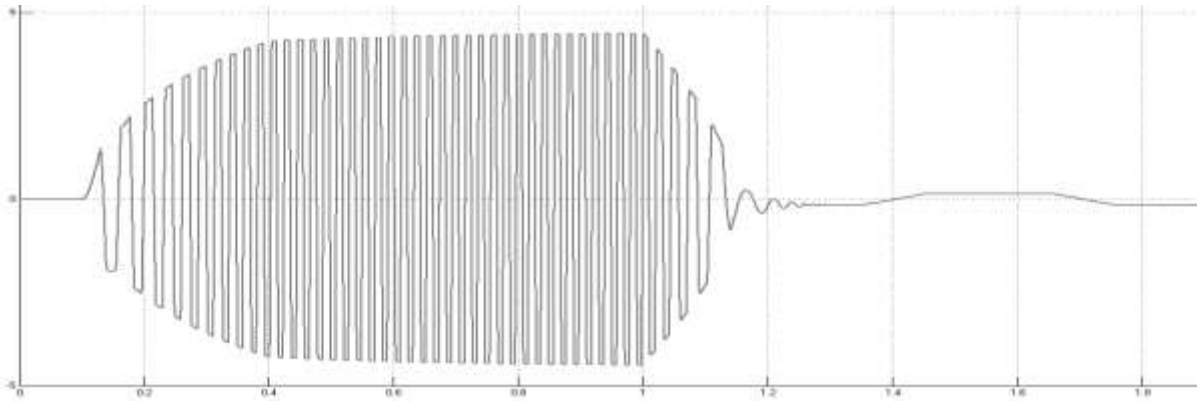

Fig. 3-14. Line to line back EMF (V)

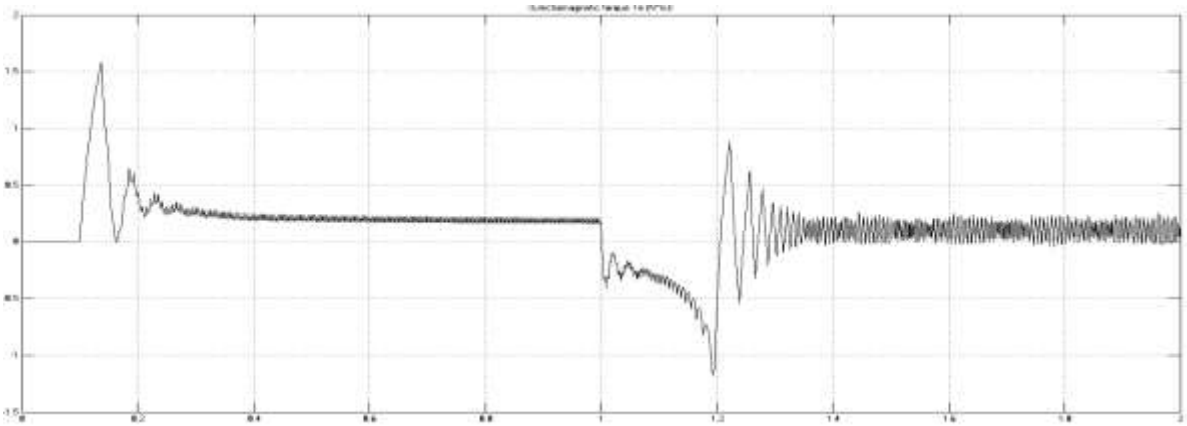

Fig. 3-15. Electromagnetic torque generated

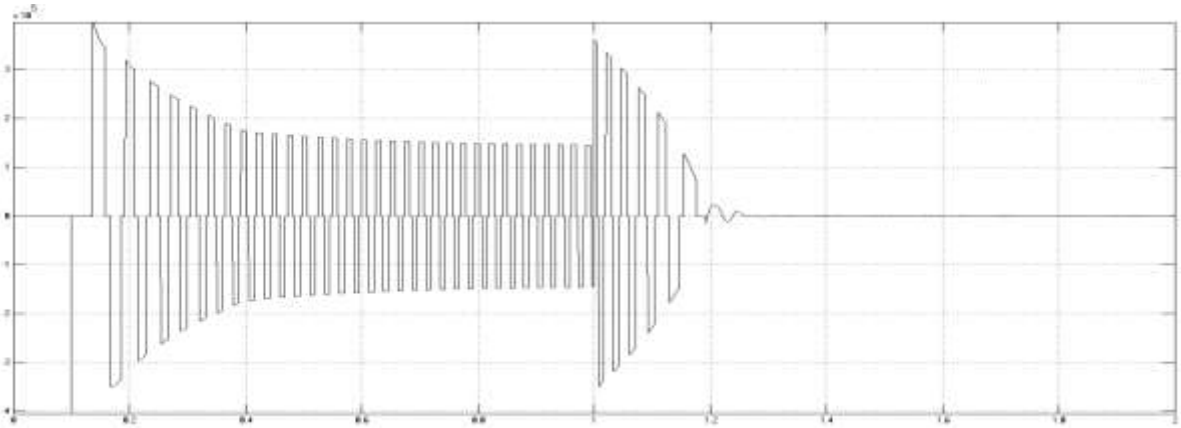

Fig. 3-16. Current reference generated

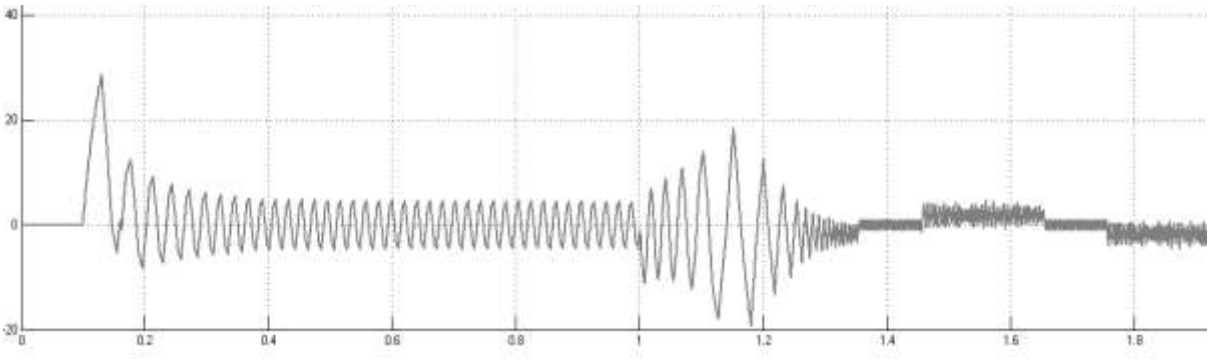

Fig. 3-17. Rotor phase current (A)

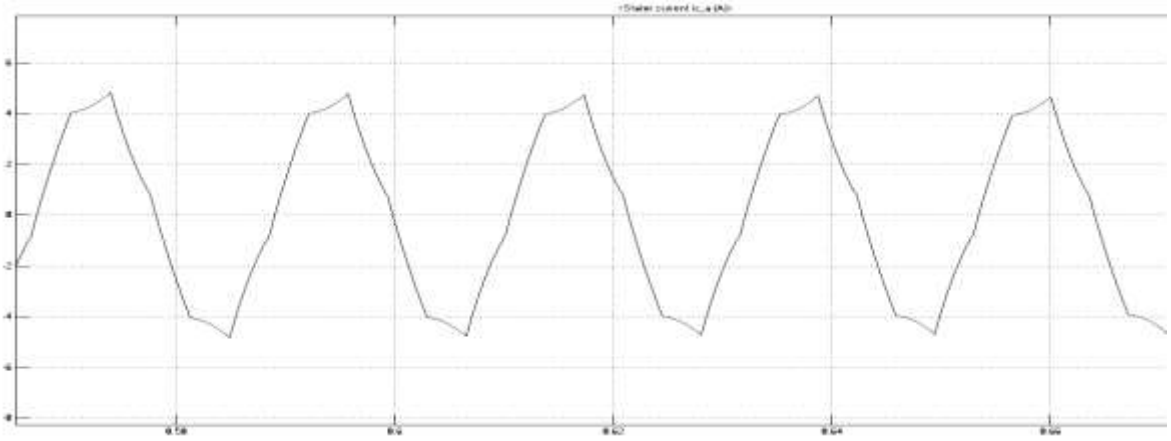

Fig. 3-18. Stator current at 1500 RPM

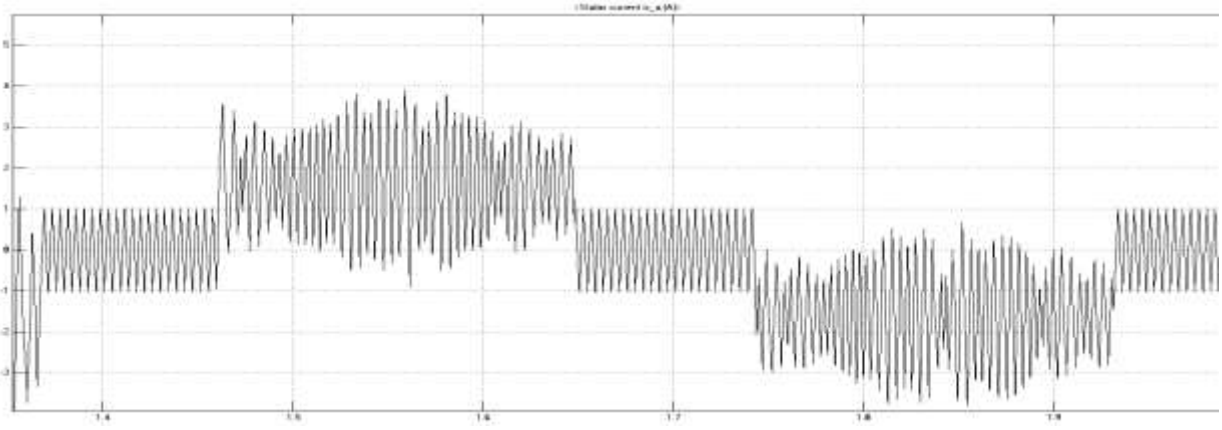

Fig. 3-19. Stator current at 50 RPM

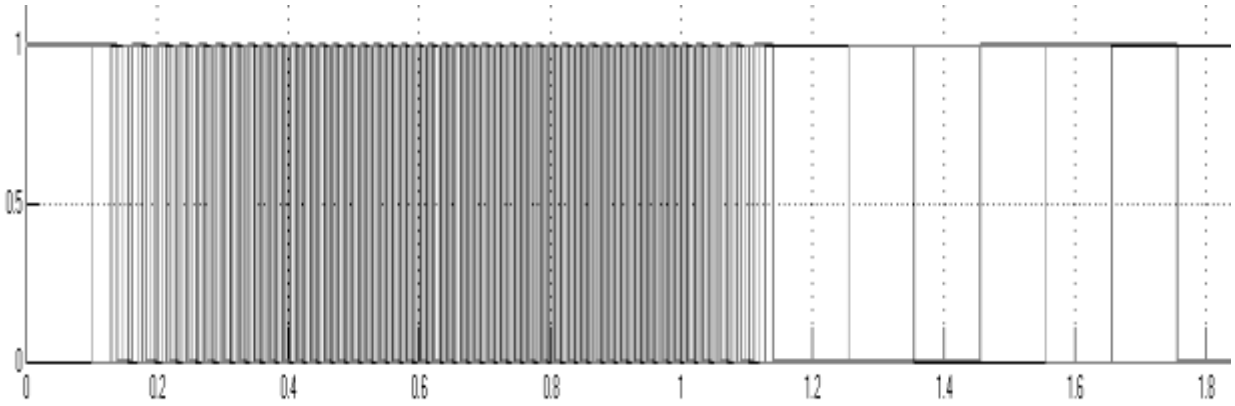

Fig. 3-20. Hall sensor signal

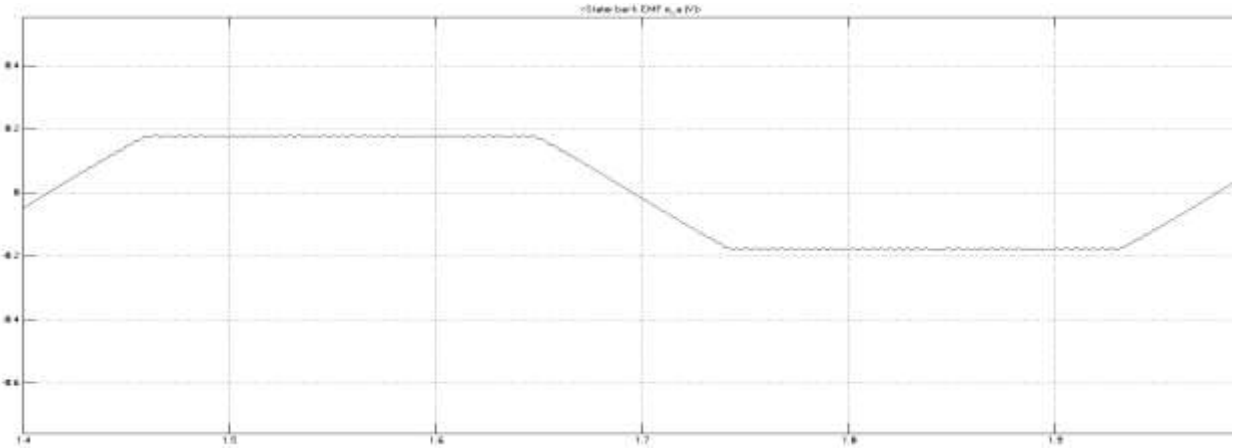

Fig. 3-21. Phase back EMF (V) at 50 RPM

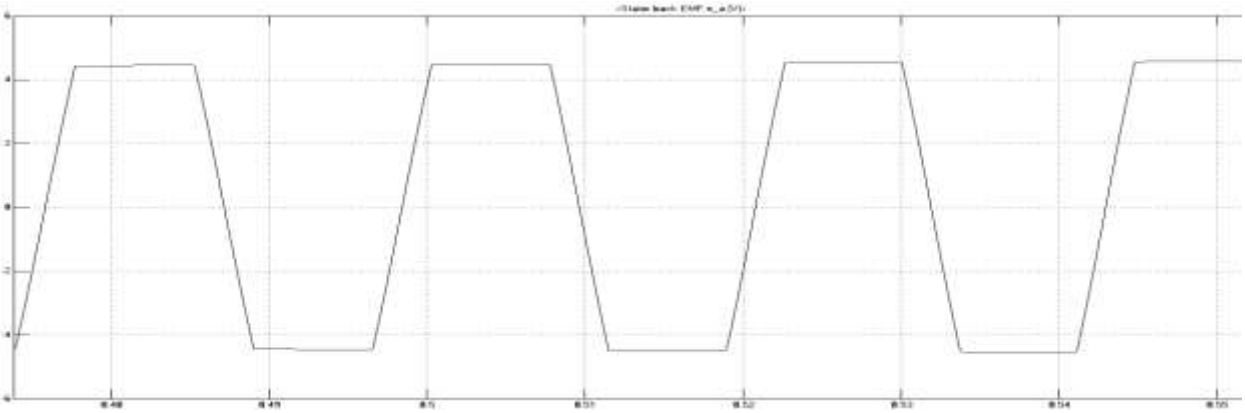

Fig. 3-22. Phase back EMF (V) at 1500 RPM

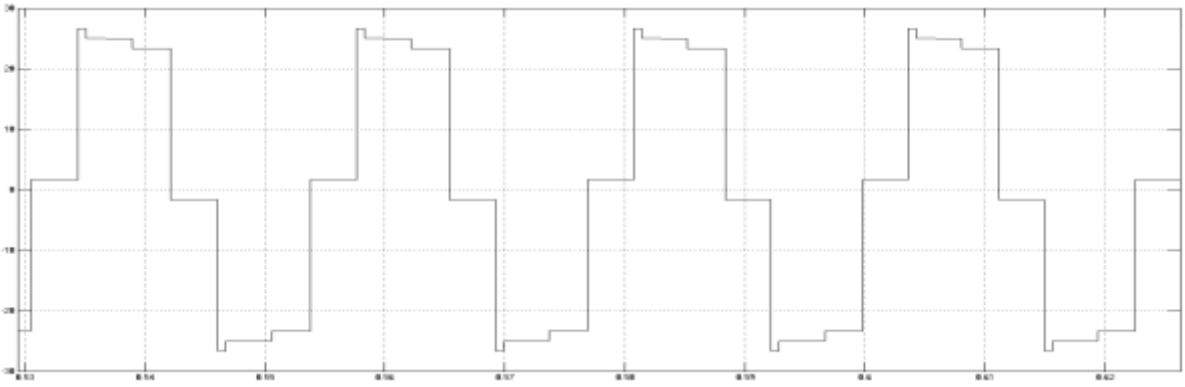

Fig. 3-23. Phase voltage generated by voltage source inverter

3.5. Experiment

The experimental setup is done in the laboratory for a 200 W, 10 A, 8000 RPM BLDC motor as shown in Fig. 3-24. A voltage source inverter is fed by six gate pulses to generate 3-phase voltage waveforms to run the BLDC motor. The control system discussed above (speed loop and current loop) is built using Simulink and ControlDesk environment and interfaced with real time using a dSPACE board. The dSPACE board is shown in Fig. 3-25.

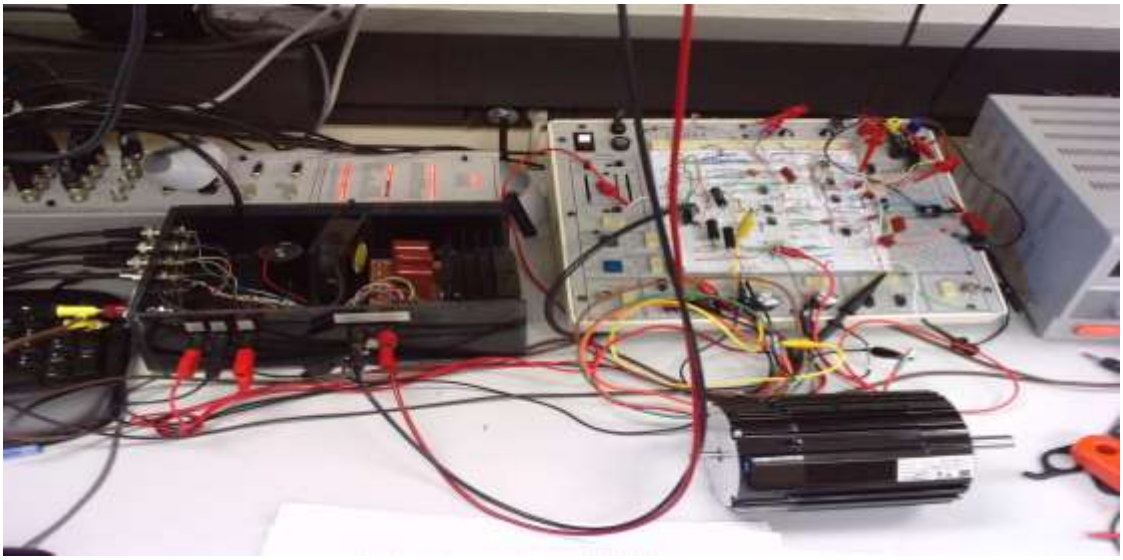

Fig. 3-24. Experimental setup for the BLDC speed control using Hall sensor

Fig. 3-25. dSPACE board used for interfacing Simulink to hardware

3.5.1. Current Measurement

Current waveforms of the three phases of the motor are measured by instrumentation amplifier, a measuring circuit and a passive low pass filter. A 0.01Ω high power resistance was used in series with each phase to measure the current. The measuring circuit is shown below in Fig. 3-26.

The reason of using a Wheatstone bridge combination instead of directly feeding the terminals of 0.01Ω resistor to the instrumentation amplifier is to avoid common mode voltage. Typically INA128 ICs have a maximum common mode voltage of 8V. Since the dSPCE board can output voltages within only ±10 V, and since the terminals of the 0.01 Ω resistor can definitely experience more than 8 volts, a voltage divider combination is necessary to avoid common mode voltages in the instrumentation amplifier and hence avoid measurement error.

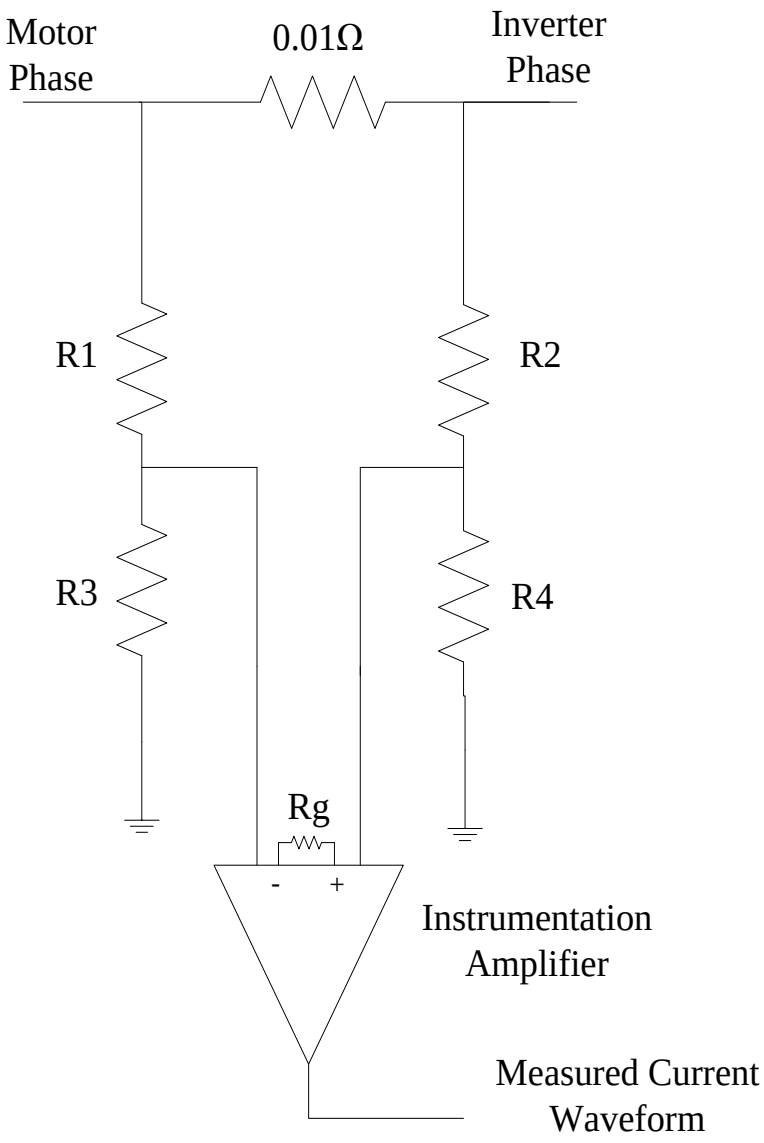

Fig. 3-26. Current measurement circuits using instrumentation amplifier

3.5.2. Speed Measurement

No external speed sensor was used for speed measurement of the BLDC motor. The hall effect sensor provide square wave signals which have same frequency as the frequency of the rotor. Thus, speed was extracted from hall signals with the following Simulink diagram below.

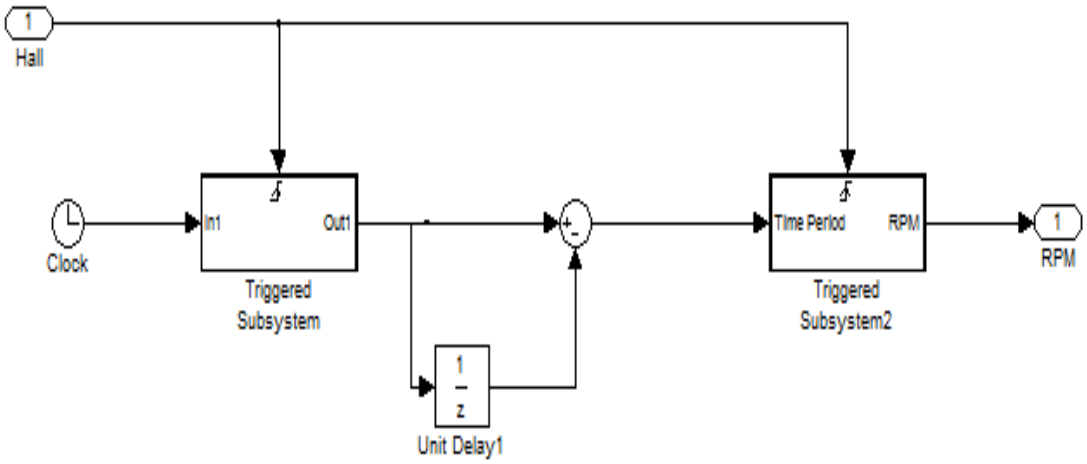

Fig. 3-27. Speed measurement from Hall sensor information

3.5.3. Key Experimental Waveforms

Experimental results obtained from the previous setup are shown in the following figures (Fig. 3-28, Fig. 3-29, Fig. 3-30, Fig. 3-31, Fig. 3-32) for a step speed command of 4000 RPM to 2000 RPM. All results are obtained via Simulink, ControlDesk and dSPACE.

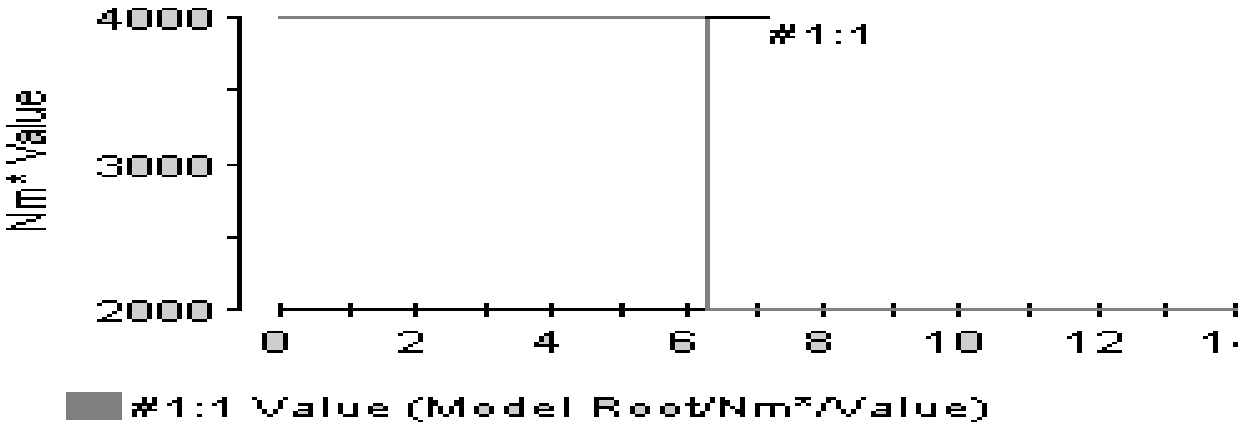

Fig. 3-28. Speed command

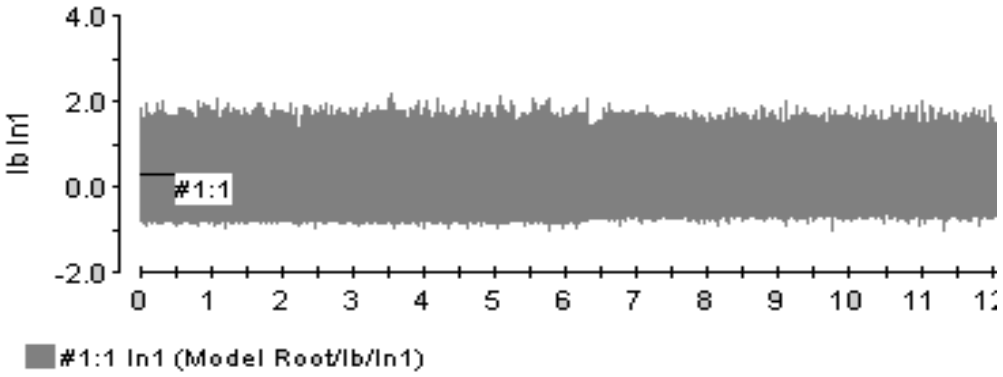

Fig. 3-29. Phase current

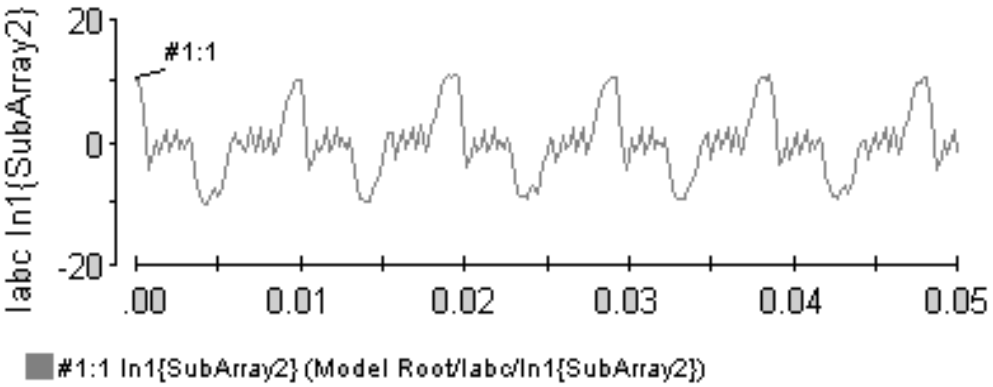

Fig. 3-30. Phase current (zoomed)

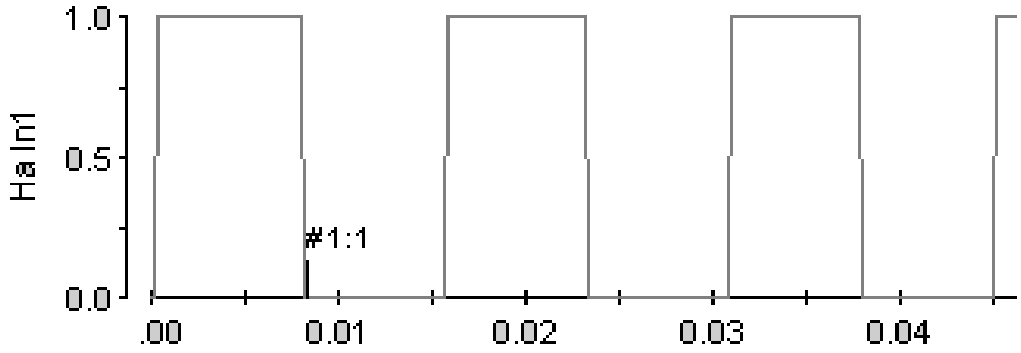

Fig. 3-31. Hall sensor signal

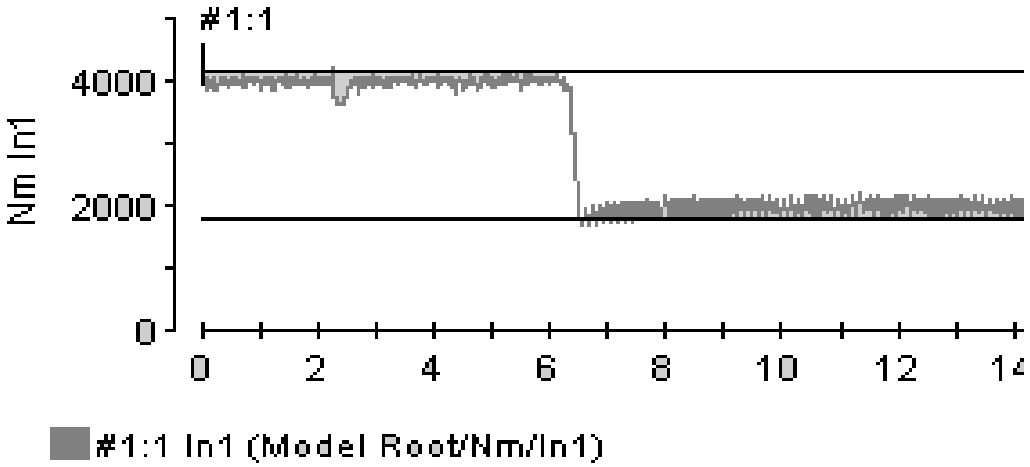

Fig. 3-32. Measured speed

As shown in Fig. 3-32, motor speed is regulated perfectly according to the commanded speed.

3.6. Conclusion

In this chapter, the complete mathematical model of Brushless DC motor has been presented along with individual loop control schemes, i.e. current and speed control schemes. A typical BLDC motor drive with mounted hall effect sensors has been discussed with six step inverter. Simulation result has been presented for speed control and laboratory experimental results were included to validate the simulation and theory.

CHAPTER 4. SENSORLESS CONTROL OF BRUSHLESS DC MOTOR

In this chapter, a review of the state of the art research works on sensorless control of BLDC motor will be given. Then a novel sensorless control scheme based on state observer and noise insensitive commutation scheme will be discussed. Simulation result will be provided to validate the idea at the end.

As discussed in Chapter 1, there are several sensorless control methods proposed in the last three decades. Some of them require the sensing of back EMF. Many of them have problems with low speed operations. Although a significant amount of research has been done for overcoming the low speed operation issue, methods and techniques are still being researched for improving low speed operation. Among the several sensorless control methods, back EMF sensing and detection is the one that this thesis is concerned about.

4.1. Direct Back EMF Detection

Generally, three phase brushless DC motors are operated in the six-step 120° commutation mode. That means, at any certain time, only two of the three phases are conducting and the other phase is un-energized. For instance, if phases A and B are conducting current, phase C will be floating and unexcited. The conduction interval takes 60 electrical degrees and referred to as a step, and hence the name six-step. Commutation means the transition from one state to another during operation. Fig. 4-1 shows [5] the six steps of the inverter and their transition.

The first step is called AB, then AC, BC, BA, CA, CB and then repeating. It is important to note that the step names are made from phases having positive to negative states.

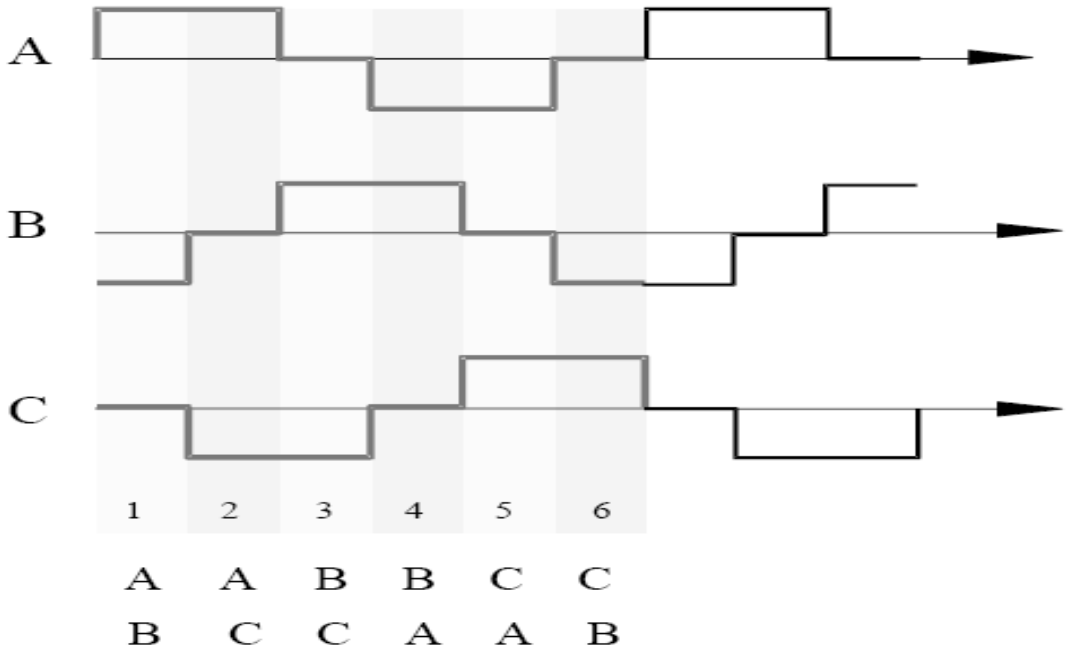

Fig. 4-1. Typical six step waveforms of a BLDC motor

It is discussed earlier that for maximum power and torque output, the current is commutated in a way that the current is in exact phase with the back EMF during the steady state mode. Rotor position determines when to commutate the current. In a sensorless control method, no physical sensor can be used for position detection, so other means have to be implemented for rotor position detection. Since the shape of the back EMF changes depending on the rotor position, it is quite possible to determine the commutation by having a back EMF detection circuitry. In Fig. 4-2, the back EMF is shown with along with the phase current [5]. It is evident that if the zero crossing of the back EMF can be determined, we can find when to commutate the current exactly.

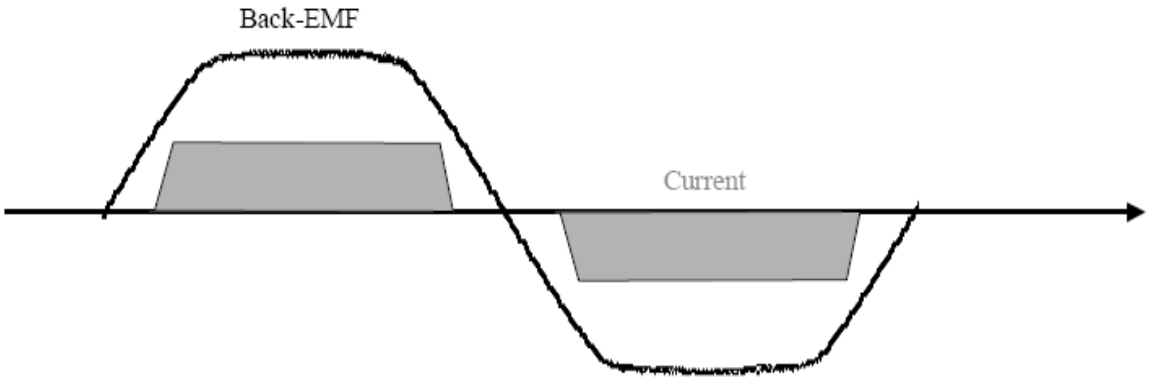

Fig. 4-2. Phase back EMF and current

Since one of the three phases does not conduct any current at a certain time, this gives a chance to measure the zero crossing of the back EMF. Fig. 4-3 illustrates this concept [5].

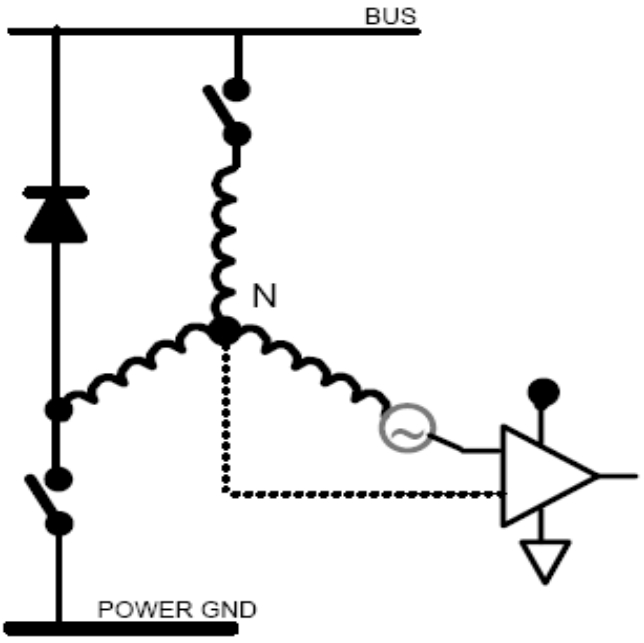

Fig. 4-3. Phase voltage measurement with respect to motor neutral point [5]

The voltage of the un-energized phase has to be measured which needs the motor neutral point to be identified because phase voltage is basically the voltage of the phase with respect to the neutral point, which is usually not the inverter ground. Since most Y-connected motors have their neutral point unexposed, it is physically not possible to identify the motor neutral and measure the phase voltage. Hence, in practice, a method of creating a virtual neutral point is most commonly used. Theoretically, the virtual neutral point will have the same potential as of the actual neutral point if the motor is perfectly balanced [5] The virtual neutral point is created by three identical resistors as shown in (4.4) & (4.5).

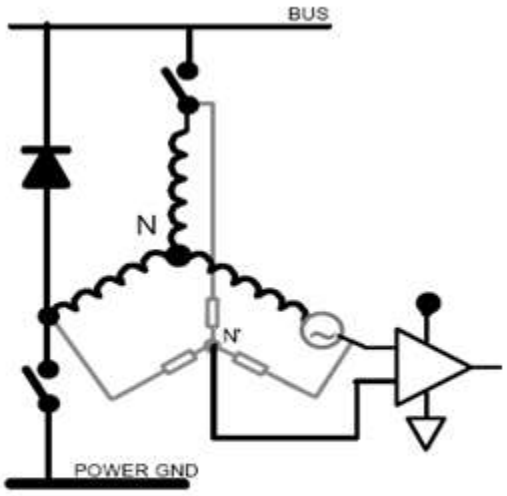

Fig. 4-4. zero crossing detection scheme with virtual neutral point

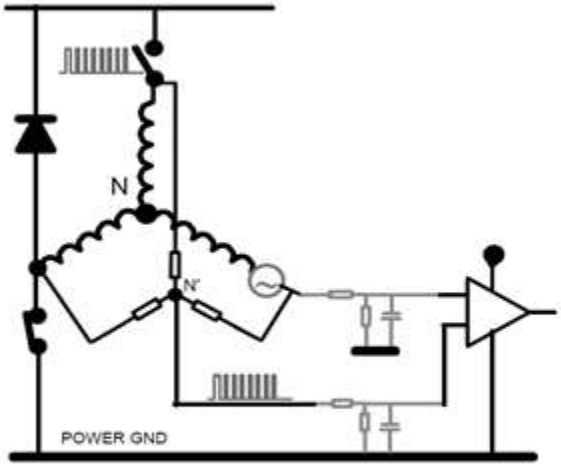

Fig. 4-5. Use of voltage divider & filter in neutral point based back EMF detection scheme

Once the virtual neutral point is established, it is possible to identify the zero crossing points by comparing the phase voltage with the virtual neutral point using a comparator. This method has several disadvantages [5]:

- Since the motor phases are turned on and off with a PWM signal, the neutral is not a stationary point. It's voltage ranges from the inverter ground to maximum DC bus voltage of the inverter. As a result, the common mode voltage across the comparator can be very high (from ground to DC bus voltage), which is not acceptable by the op-amp because typical common mode voltage rating of Op Amps/comparators are very small.
- In order to measure the phase voltage by avoiding the common mode voltages, a voltage dividers have to be used (Fig. 4-5) which adds complexity, attenuation and noise to the signal.
- In order to reduce noise, low pass filters are to be used which adds some operational delay in the system. The delay can make the current not properly aligning with the back EMF which eventually will disturb the commutation at high speeds.

All these issues can limit the use of this system in a narrow speed range which is a big disadvantage. In order to solve this problem, different methods have been proposed. One of the most effective methods was to find out the motor neutral voltage in terms of phase back EMF and thus make a direct proportional relationship of back EMF with the measured phase voltage [5]. In this method, PWM is applied on only the high side switches of the inverter keeping the low side switches always on. The back EMF is sensed during the PWM off time. This idea is illustrated in Fig. 4-6 in which the inverting input terminal of the op amp is not at virtual ground.

In this method, since one of the power poles experience PWM and the other one is always on, at a certain time only one of the six switches is turned on. When the upper switch of a phase, let's say A is turned on, current will be flowing from, let's say, winding A to B and

freewheeling through the diode parallel to the bottom transistor of phase A during the upper transistor off time. The equivalent circuit is shown in Fig. 4-7.

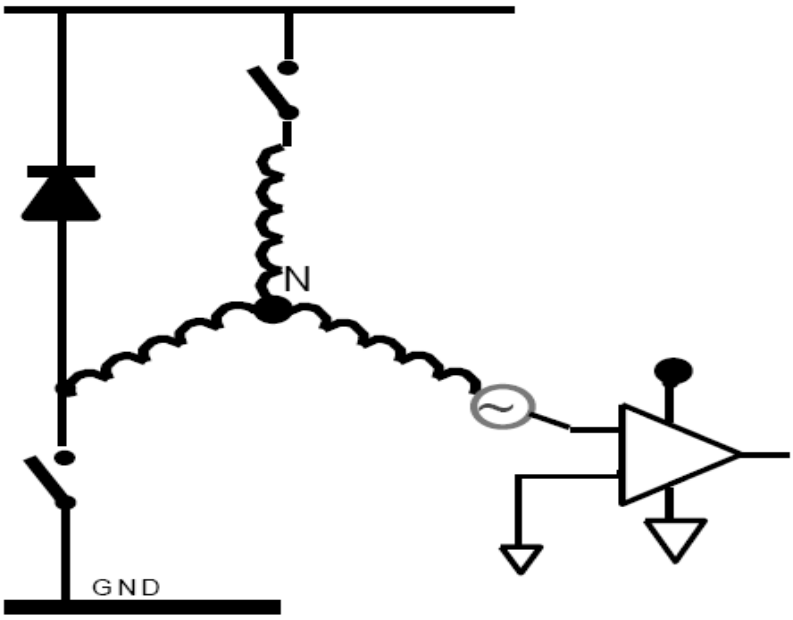

Fig. 4-6. Improved back EMF zero crossing detection

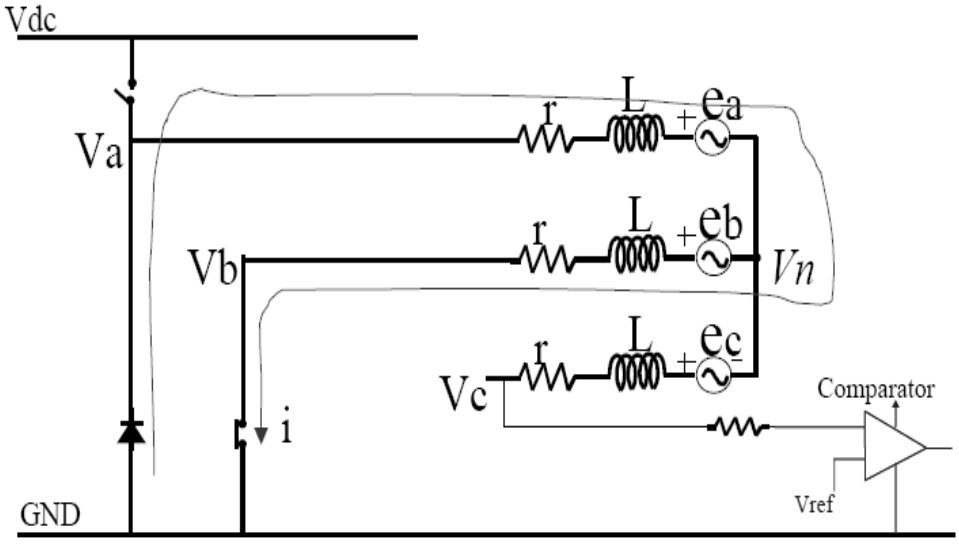

Fig. 4-7. Back EMF detection during PWM off time in direct back EMF sensing method

In the circuit above, ignoring the voltage drop in the diode,

$$V_n = 0 - ri - L\frac{di}{dt} - e_a \tag{4.1}$$

$$Vn = ri + L\frac{di}{dt} - eb \tag{4.2}$$

From (4.1) and (4.2), we get

$$V_n = -\frac{e_a + e_b}{2} \tag{4.3}$$

Since we are assuming balanced condition, $e_a + e_b + e_c = 0$.

So, equation (4.3) becomes

$$V_n = \frac{e_c}{2} \tag{4.4}$$

and the phase voltage becomes

$$V_c = e_c + V_n = \frac{3}{2} e_c \tag{4.5}$$

From equation (4.5), it is evident that in this scheme it is possible to find out the exact value of the instantaneous back EMF from the measured line voltage at that instant. This method works regardless of noise and floating neutral point. This improved scheme is simple and it does not suffer from attenuation due to voltage dividers and delay due to low pass filters.

As discussed briefly in Chapter 1, there are some other methods of creating the commutation of currents. One of the methods is third harmonic back EMF sensing method [15]. It is attractive because of its simplicity and low cost, but the relatively low value of the third harmonic is a big problem in the low speed range.

Another method is to use back EMF integration technique. In this method, the rotor position is found by integrating the back EMF of the silent phase. When the un-energized phase's back-EMF (measured by measuring the terminal voltage) crosses zero, the integration starts and when it crosses a pre-set threshold, the integration stops. This corresponds to a commutation instant. This method is good in terms of switching noise sensitivity and automatic adjustment of inverter switching instants to the change in rotor speed. The main problem of this method is low accuracy at low speeds.

Flux linkage based technique is another method which has been researched. The basic idea behind this method is to estimate the flux linkage by integrating the applied voltage and current. After that, the rotor position can be calculated using its initial value, flux linkage's relationship to rotor position and machine parameters. The problem with this method is, at low speeds the integration takes a long time, and inaccurate sampled current makes the error significant.

Some research has been done for estimating the rotor position information based on the conducting state of the free-wheeling diode in the un-energized phase. A small amount of current of the silent phase starts flowing through the free-wheeling diode of the inverter, which actually corresponds to a point when back EMF crosses zero. This method also has the problem of large error at low speeds. In addition, the need for additional isolated power supplies makes this system complex.

4.2. Speed Insensitive Commutation Function Based Back EMF Detection Method

Most of the methods described in the previous section have the limitation of poor performance in the low speed range. The reason for the poor performance in that zone is, that the

back EMF is a speed dependent function, and once the speed becomes very low or zero, it becomes harder to measure the back EMF accurately and perform the commutation. That is why it is not possible to use speed dependent back EMF sensing method, at least in the low speed range. Another important drawback is, the commutation point is supposed to be 30° shifted from the back EMF zero crossing, which can be accurately estimated in the steady state but has significant error in the dynamic region. In order to overcome this problem, a novel method was proposed in 2004 by Kim & Ehsani [17] which resolves the speed dependency problem of the back EMF sensing method and makes the BLDC drive completely rotor speed independent. To illustrate the idea behind this method, let's consider the BLDC motor drive in Fig. 4-8.

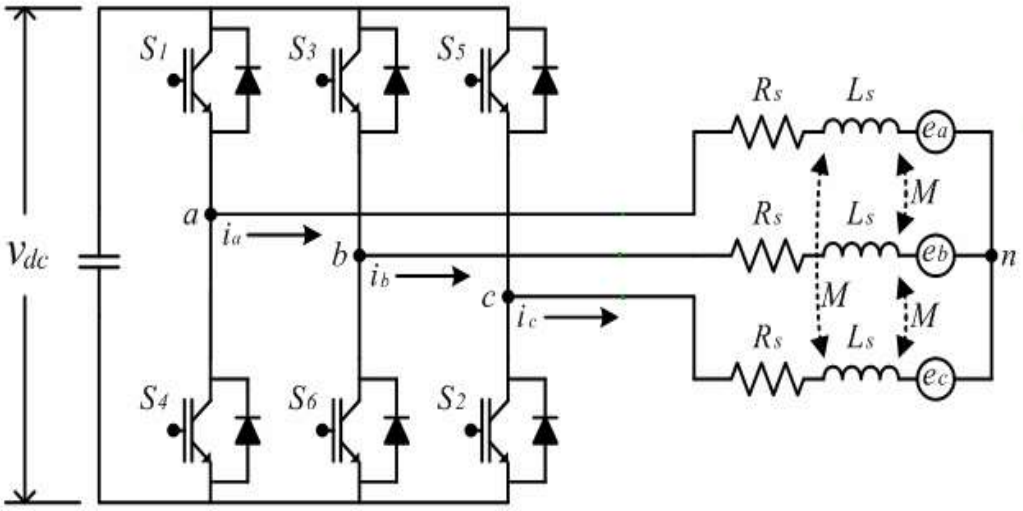

Fig. 4-8. Power circuit of a BLDC motor drive system [18]

From Fig. 4-8, the individual phase equations can be written from equations (2.10), (2.11) and (2.12) as follows:

$$V_{an} = i_a R_s + L\frac{d}{dt}i_a + e_{an} \quad (4.6)$$

$$V_{bn} = i_b R_s + L\frac{d}{dt}i_b + e_{bn} \quad (4.7)$$

$$V_{cn} = i_c Rs + L\frac{d}{dt}i_c + e_{cn} \quad (4.8)$$

where

R is the stator resistance, L is the combined inductance, and

V_{an} ,V_{bn} & V_{cn} are the applied phase voltages.

Subtracting (4.7) from (4.6), the line to line voltage V_{ab} is found as

$$V_{ab} = V_{an} - V_{bn} = (i_a - i_b) R_s + L\frac{\mathbf{d}}{\mathbf{dt}}(i_a - i_b) + e_{an} - e_{bn}) \quad (4.9)$$

From (4-9), the back EMF difference can be found as

$$e_{an} - e_{bn} = V_{an} - V_{bn} - (i_a - i_b) R_s - L\frac{\mathbf{d}}{\mathbf{dt}}(i_a - i_b) \quad (4.10)$$

Subtracting (4.8) from (4.7) leads to another equation as follows:

$$e_{bn} - e_{cn} = V_{bn} - V_{cn} - (i_b - i_c) R_s - L\frac{\mathbf{d}}{\mathbf{dt}}(i_b - i_c) \quad (4.11)$$

Taking $e_{an} - e_{bn} = e_{ab}$, $e_{bn} - e_{cn} = e_{bc}$, $V_{an} - V_{bn} = V_{ab}$ and $V_{bn} - V_{cn} = V_{bc}$, the following equations can be written:

$$e_{ab} = V_{ab} - (i_a - i_b) R_s - L\frac{d}{dt}(i_a - i_b) \quad (4.12)$$

$$e_{bc} = V_{bc} - (i_b - i_c) Rs - L\frac{\mathbf{d}}{\mathbf{dt}}(i_b - i_c) \quad (4.13)$$

We know from equation (2.14) that,

$$e_{an} = k_e * \omega_e * f_a(\theta) \tag{4.14}$$

$$e_{bn} = k_e * \omega_e * f_b(\theta) \tag{4.15}$$

and

$$e_{cn} = k_e * \omega_e * f_c(\theta) \tag{4.16}$$

where, k_e refers to motor back EMF constant, ω_e is the electrical speed of the rotor and $f(\theta)$ is the rotor position function which has the same shape as the motor back EMF of the corresponding with a maximum magnitude of 1.

Subtracting (4-15) from (4-14)

$$e_{an} - e_{bn} = k_e*\omega_e*(f_a(\theta) - f_b(\theta)) \tag{4.17}$$

Taking $fa(\theta) - fb(\theta) = fab(\theta)$, equation (4-17) can be re-written as

$$eab = k_e*\omega_e*f_{ab}(\theta) \tag{4.18}$$

Similarly, the subtraction of (4-16) from (4-15) gives

$$e_{bc} = k_e*\omega_e*f_{bc}(\theta) \tag{4.19}$$

From (4-12) and (4-18), the following equation is obtained:

$$V_{ab} - (i_a - i_b) R_s - L\frac{d}{dt}(i_a - i_b) = k_e * \omega_e * f_{ab}(\theta), \text{ Or,}$$

$$f_{ab}(\theta) = \frac{\mathbf{1}}{\mathbf{k_e}* \omega_\mathbf{e}} * V_{ab} - (i_a - i_b) R_s - L\frac{\mathbf{d}}{\mathbf{dt}}(i_a - i_b) \tag{4.20}$$

Similarly, from (4-13) and (4-19), the following equation is obtained:

$$f_{bc}(\theta) = \frac{\mathbf{1}}{\mathbf{k_e}* \omega_\mathbf{e}} * V_{bc} - (i_b - i_c) R_s - L\frac{\mathbf{d}}{\mathbf{dt}}(i_b - i_c) \tag{4.21}$$

Both equations (4.20) and (4-21) are functions of speed. Hence, if the rotor position has to be calculated from these two equations, that will be inefficient at low speeds because speed estimation is difficult at low speeds due to error in back EMF estimation. In other words, the speed dependency of back EMF sensing at low speeds makes rotor position estimation difficult. This problem can be solved by dividing equation (4-21) by (4-20) giving

$$\frac{f_{bc}(\theta)}{f_{ab}(\theta)} = \frac{(V_{bc} - (i_b - i_c)Rs - 2L\frac{di_{bc}}{dt})}{(V_{ab} - (i_a - i_b)Rs - 2L\frac{di_{ab}}{dt})} \tag{4.22}$$

Since $\frac{f_{bc}(\theta)}{f_{ab}(\theta)}$ has a direct one to one relationship with rotor position, it is possible to find the rotor position from this function. The plot of $\frac{f_{bc}(\theta)}{f_{ab}(\theta)}$ with respect to θ is shown in Fig. 4-9.

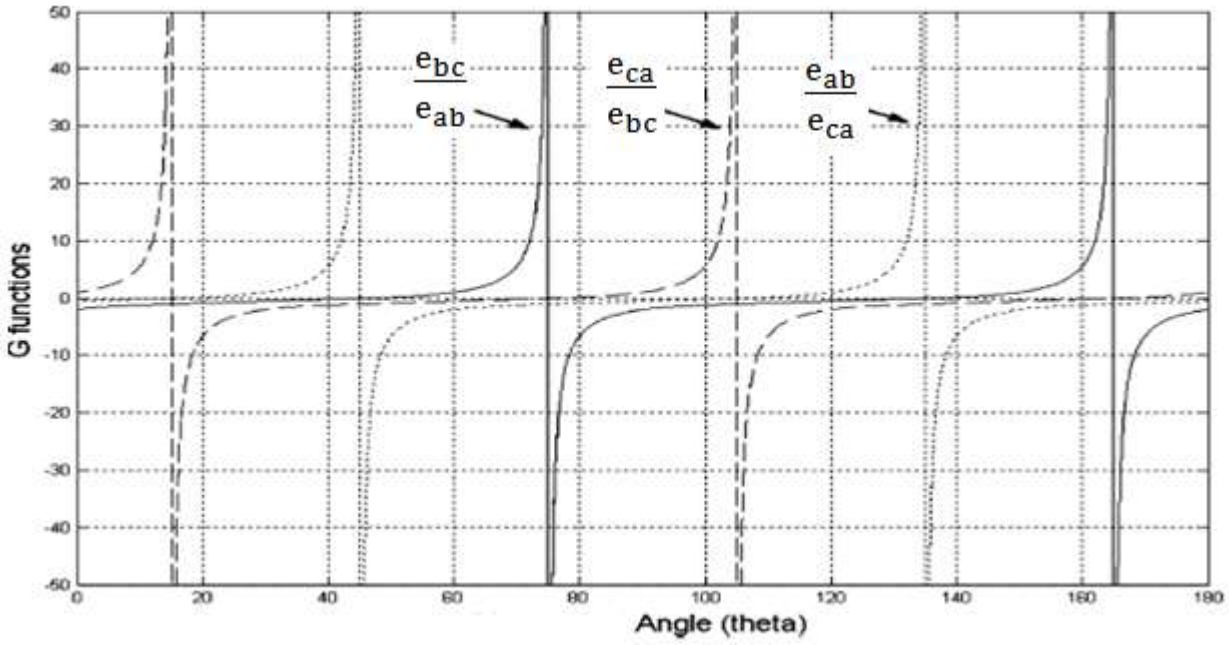

Fig. 4-9. Plot of $\frac{f_{bc}(\theta)}{f_{ab}(\theta)}$ with respect to angle

The standard commutation instant is when the curves reach infinity, i.e. when they change from positive infinity to negative infinity.

Kim & Ehsani [17] only utilized the positive part of the $\frac{f_{bc}(\theta)}{f_{ab}(\theta)}$function and thus created the commutation for the motor. They commutated the motor based on a threshold value. The threshold value is defined based on the current rising time and desired advanced angle. When the $\frac{f_{bc}(\theta)}{f_{ab}(\theta)}$function reaches that threshold value, the motor is commutated in six different modes for six step commutation, as shown in Fig. 4-10 [17]

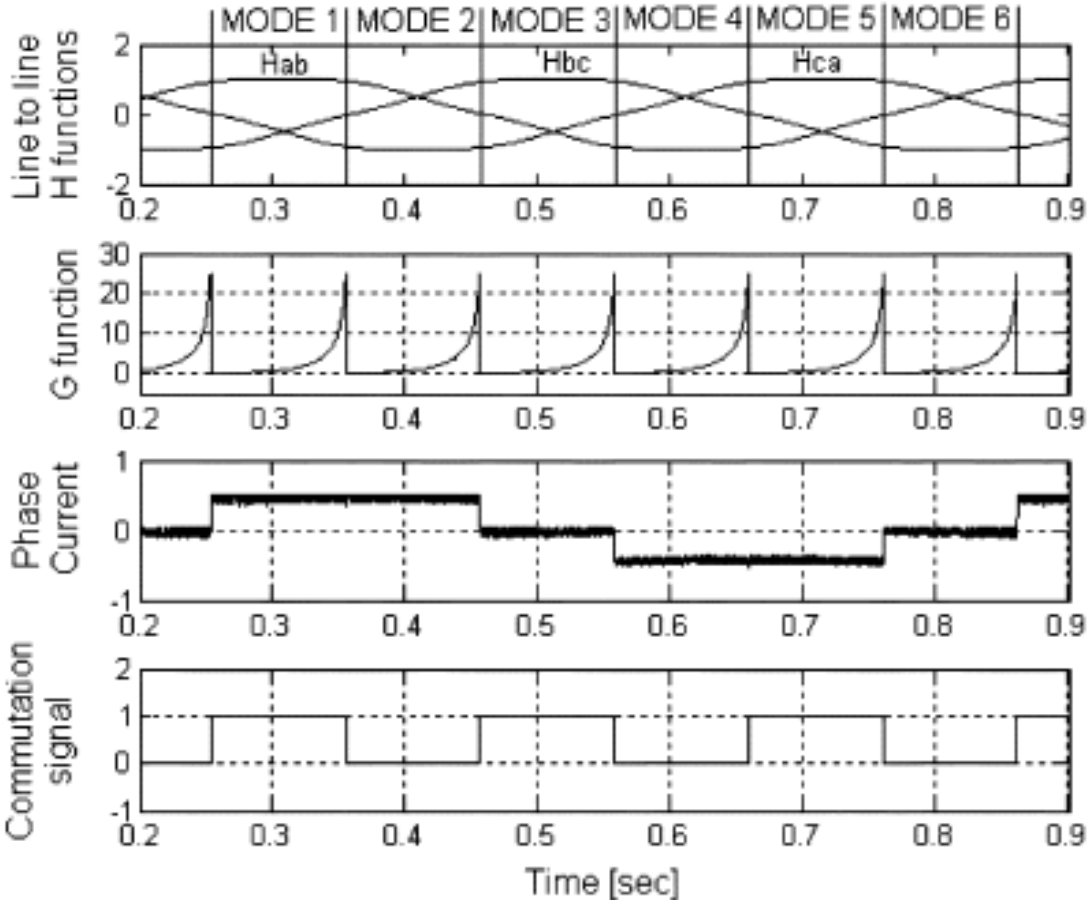

Fig. 4-10. Simulation results from the method of [17]

Table 2 shows the position estimation equations at each mode in Fig. 4-10 [17]. From Table 2, it is evident that $\frac{f_{ca}(\theta)}{f_{bc}(\theta)}$ is utilized as a position estimation equation at mode 1, whereas after 60 electrical degrees, at mode 2, $\frac{f_{bc}(\theta)}{f_{ab}(\theta)}$ is utilized, and so on. Obviously, the time difference between each mode is 60 electrical degrees.

Table 4-1. Position estimation equations from mode 1 to mode 6

Mode 1 and Mode 4	$G(\theta)_{ab} = \frac{f_{ca}(\theta)}{f_{bc}(\theta)} = \frac{V_{ca} + R\, i_{ca} + L\frac{di_{ca}}{dt}}{V_{bc} - R\, i_{bc} - L\frac{di_{bc}}{dt}}$
Mode 2 and Mode 5	$G(\theta)_{ca} = \frac{f_{bc}(\theta)}{f_{ab}(\theta)} = \frac{V_{bc} + R\, i_{bc} + L\frac{di_{bc}}{dt}}{V_{ab} - R\, i_{ab} - L\frac{di_{ab}}{dt}}$
Mode 3 and Mode 6	$G(\theta)_{bc} = \frac{f_{ab}(\theta)}{f_{ca}(\theta)} = \frac{V_{ab} + R\, i_{ab} + L\frac{di_{ab}}{dt}}{V_{ca} - R\, i_{ca} - L\frac{di_{ca}}{dt}}$

As mentioned above, Ehsani and Kim's method [17] works on threshold, i.e. when the $\frac{f_{bc}(\theta)}{f_{ab}(\theta)}$ (or $\frac{f_{ca}(\theta)}{f_{bc}(\theta)}$, or $\frac{f_{ab}(\theta)}{f_{ca}(\theta)}$ depending on commutation) function crosses the threshold. This method works well in the low speed range. The drawback of this method is if some noise affects the function $\frac{f_{bc}(\theta)}{f_{ab}(\theta)}$ (or the rest), then the motor may be commutated incorrectly. For instance, in Fig. 4-11, the motor is supposed to commutate at the points where the $\frac{f_{ab}(\theta)}{f_{bc}(\theta)}$function touches or exceeds a pre-set threshold th1. In the meantime, if a noise with a height of (1) which is less than th1 occurs, the motor will not commutate, but if a noise of height of (2) occurs, the motor will

commutate before the point where it is supposed to commutate. As a result, the motor will face unwanted commutation which may halt or destroy its operation.

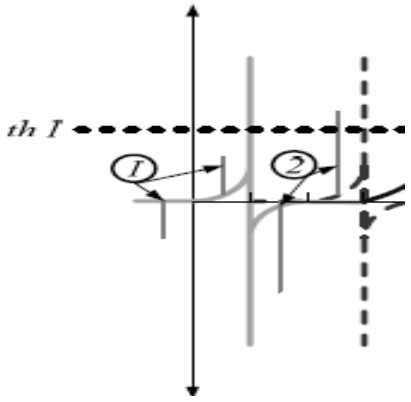

Fig. 4-11. Motor commutation affected by noise [17]

For solving this problem, several methods have been proposed and one of them is described in [18] based on state observer and dual threshold method. According to [18], $\frac{f_{ab}(\theta)}{f_{bc}(\theta)}$ (or any other commutation) was found out, and instead of one or two thresholds, three thresholds were used, as shown in Fig. 4-12. In this method, the commutation will only occur if the function $\frac{f_{ab}(\theta)}{f_{bc}(\theta)}$ satisfies the condition of crossing both th1 and th3, avoiding the chance of malfunction.

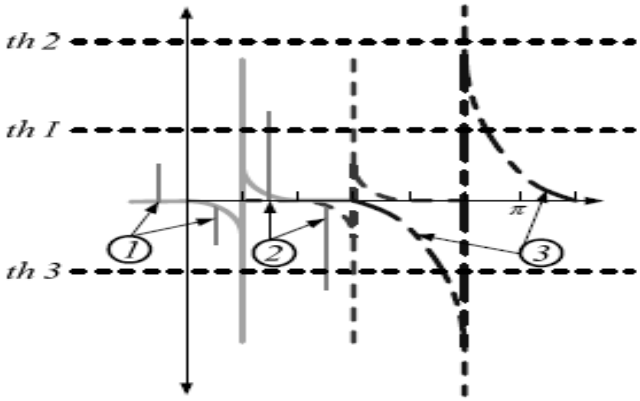

Fig. 4-12. Method proposed by [18]

4.3. Noise Insensitive Commutation Method with Observer Based Back EMF Sensing

In this thesis, a noise insensitive commutation method is proposed using the observer based back EMF sensing technique presented in [18]. The method starts with the design of the observer, as described below.

4.3.1. Mathematical Analysis

Referring to Fig. 3-1, it is found that at any 60° commutation period, only two of the phases are energized and the other phase current remains zero. Moreover, one of the conducting phase current is 180° out of phase with the other conducting phase. That simply means, one of the phase currents is entering to the neutral and the other is leaving neutral. The idea is illustrated in Fig. 4-13.

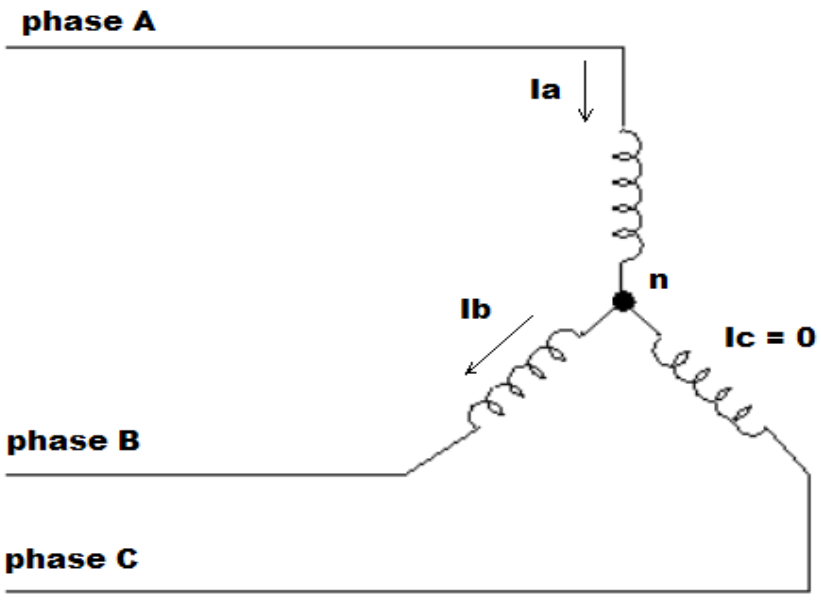

Fig. 4-13. Typical BLDC motor phase excitation at a particular instant

Assuming a balanced three phase system and peak value of the phase currents same ($i_a = i_b = i_c = i$), the total current flowing through the motor at any commutation instant becomes $i_a – (- i_b) = 2*i = 2*i_{ab}$, where $i_{ab} = i$.

This value when used in equation (4.12) gives

$$V_{ab} = 2i_{ab}R_s + 2L\frac{di_{ab}}{dt} + e_{ab} \tag{4.23}$$

Rearranging (4.23), we get

$$\frac{di_{ab}}{dt} = -\frac{e_{ab}}{2L} - \frac{2i_{ab}R_s}{2L} + \frac{V_{ab}}{2L} \tag{4.24}$$

In equation 4-24), i_{ab} and V_{ab} can be measured, that is why they are called known state variables. But e_{ab} cannot be measured so it is referred as unknown state variable. Equation (4.24) can be written as [5]

$$\dot{x} = Ax + Bu + Dv \tag{4.25}$$

$$y = Cx \tag{4.26}$$

where,

$A = [-\frac{2R_s}{2L}]$, $B = [\frac{1}{2L}]$, $D = [-\frac{1}{2L}]$,, $x = [i_{ab}]$, $u = [V_{ab}]$, $v = [e_{ab}]$, $y = [i_{ab}]$, $C = [1]$.

The back EMF here is considered as unknown disturbance. Typically, unknown disturbances can be represented by differential equations. In [18], since no experimental data is available for disturbance, the unknown disturbance is modeled by the general completely observable dynamic system. Then the entire system can be represented by an augmented

equation that models the back EMF in the form of a differential equation. The augmented model is described by the following equations:

$$\dot{x} = Ax + Bu \tag{4.27}$$

$$y = Cx \tag{4.28}$$

where $A = \begin{bmatrix} \frac{-2R_s}{2L} & \frac{-1}{2L} \\ 0 & 0 \end{bmatrix}$; $B = \begin{bmatrix} \frac{1}{2L} \\ 0 \end{bmatrix}$;

$x = \begin{bmatrix} i_{ab} \\ e_{ab} \end{bmatrix}$; u =[$V_{ab}$], y = [$i_{ab}$], C = [1 0];

The observability matrix of this system described by equations (4.27) and (4.28) is $\begin{bmatrix} 1 & 0 \\ \frac{2R_s}{2L} & \frac{-1}{2L} \end{bmatrix}$, which has a rank of 2. So it can be safely stated that the system is completely observable, a*n*d a state observer can be added to the system. The following observer is composed for the system:

$$\hat{\dot{x}} = Ax + Bu + K(y - \hat{y}) \tag{4.29}$$

where $\hat{x}$ is the observed value of the state variables and $\hat{y}$ is the observed value of the output which, in this case, is the line to line current. K is the gain matrix for the observer and it can be chosen carefully in a trial and error basis or by solving it. Careful selection of K can lead to accurate estimation of the line to line back EMF of the motor.

Therefore, the equation of whole observer including all of three phases is given by (4.30) [18].

Fig. 4-14 shows the block diagram of the proposed back EMF observer with the line to line voltage as the observer input and the line to line current and back EMF as observed outputs.

$$\frac{d}{dt}\begin{bmatrix} \hat{i}ab \\ \hat{e}ab \\ \hat{i}bc \\ \hat{e}bc \\ \hat{i}ca \\ \hat{e}ca \end{bmatrix} = \begin{bmatrix} -\frac{2Rs}{2L} & -\frac{1}{2L} & 0 & 0 & 0 & 0 \\ 0 & 0 & 0 & 0 & 0 & 0 \\ 0 & 0 & -\frac{2Rs}{2L} & -\frac{1}{2L} & 0 & 0 \\ 0 & 0 & 0 & 0 & 0 & 0 \\ 0 & 0 & 0 & 0 & -\frac{2Rs}{2L} & -\frac{1}{2L} \\ 0 & 0 & 0 & 0 & 0 & 0 \end{bmatrix} \begin{bmatrix} \hat{i}ab \\ \hat{e}ab \\ \hat{i}bc \\ \hat{e}bc \\ \hat{i}ca \\ \hat{e}ca \end{bmatrix}$$
$$+ \begin{bmatrix} \frac{1}{2L} & 0 & 0 \\ 0 & 0 & 0 \\ 0 & \frac{1}{2L} & 0 \\ 0 & 0 & 0 \\ 0 & 0 & \frac{1}{2L} \\ 0 & 0 & 0 \end{bmatrix} \begin{bmatrix} vab \\ vbc \\ vca \end{bmatrix} + \begin{bmatrix} k1 & 0 & 0 \\ k2 & 0 & 0 \\ 0 & k3 & 0 \\ 0 & k4 & 0 \\ 0 & 0 & k5 \\ 0 & 0 & k6 \end{bmatrix} \begin{bmatrix} iab - \hat{i}ab \\ ibc - \hat{i}bc \\ ica - \hat{i}ca \end{bmatrix}. \quad (4.30)$$

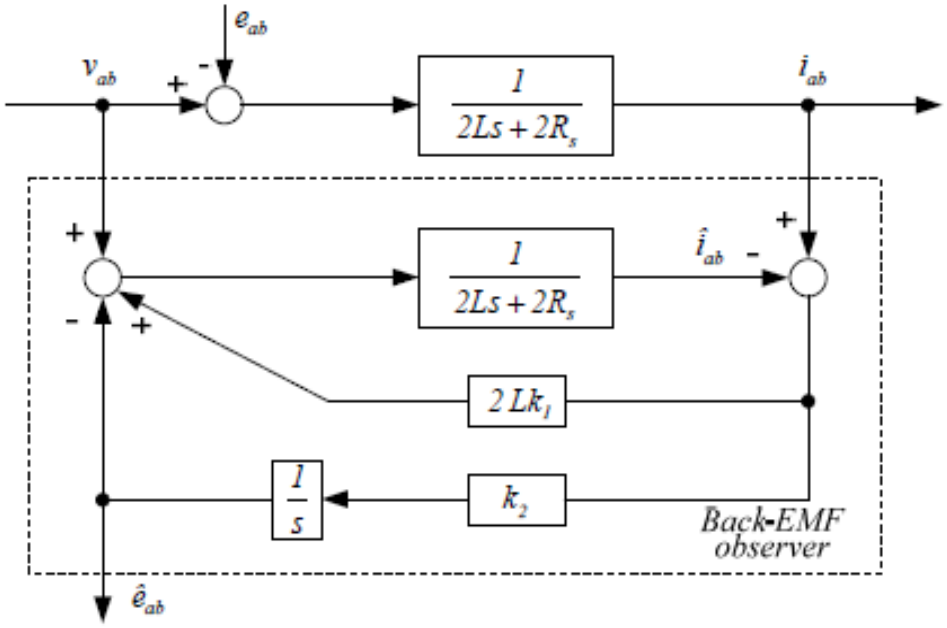

Fig. 4-14. Block diagram for the back EMF sensing equation proposed in [18]

Fig. 4-15 shows all the three phases with voltage and current as observer inputs and back EMF as output.

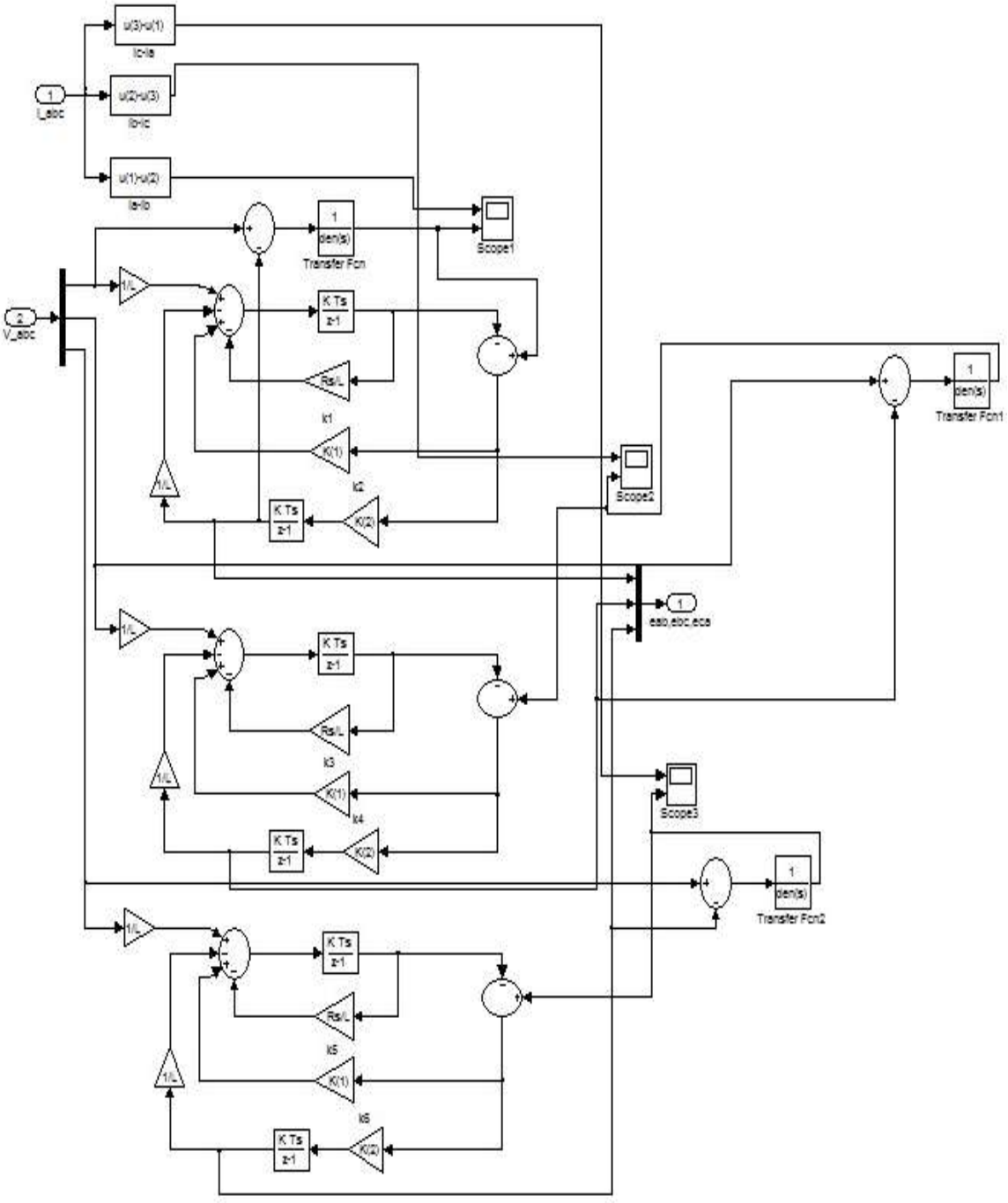

Fig. 4-15. Proposed algorithm in [18]for all three phases

Fig. 4-16 shows the comparison between actual back EMF and observed back EMF from this proposed method.

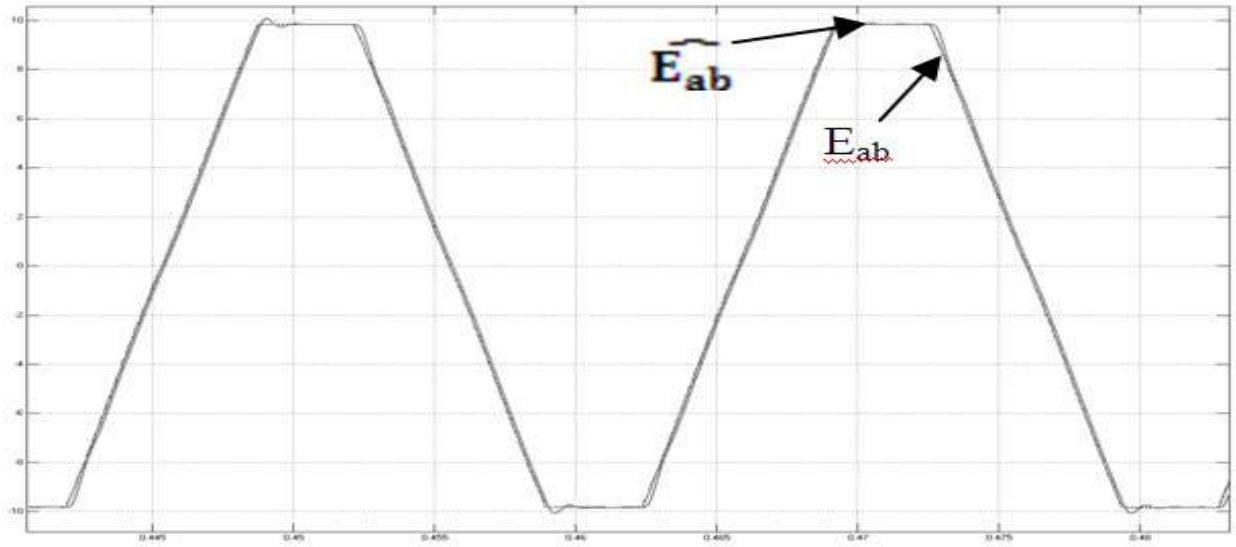

Fig. 4-16. Observed and actual line to line back EMF

The $\frac{f_{ca}(\theta)}{f_{bc}(\theta)}$function is plotted with respect to time in Fig. 4-17.

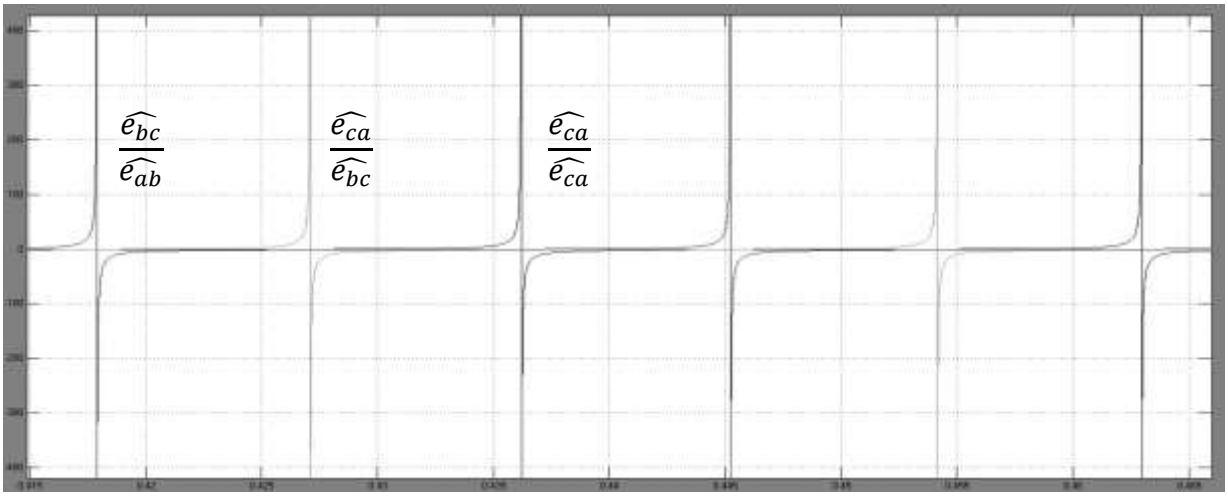

Fig. 4-17. Plot of $\frac{\mathbf{f_{ca}(\theta)}}{\mathbf{f_{bc}(\theta)}}$ as a function of angle

4.3.2. **Commutation**

In [17] and [18], a threshold based commutation signal has been proposed. Although the method proposed in [17] works good for low speeds, it is not noise free. The noise affects the commutation since the method is threshold based. Even though the method proposed in [18] overcomes the noise problem to some extent by introducing three thresholds, it can still be affected by noise. This problem can be totally eliminated by introducing a commutation process based on electrical angle. From simulation and careful observation it is found that the commutation function defined as $\frac{f_{bc}(\theta)}{f_{ab}(\theta)}$ is a tangent function. Thus, instead of using any threshold to avoid noise, in this thesis the commutation function is defined as

$$G(\theta) = \tan\theta = \frac{f_{bc}(\theta)}{f_{ab}(\theta)}$$

Or ,

$$\theta = \tan^{-1} G(\theta) \tag{4.31}$$

where, $\theta = \omega_e t$.

Thus the rotor position can be accurately estimated using equation (4.31). The advantage of this equation is that it can accurately measure the commutation point in the presence of any noise; hence the method is less noise sensitive than the ones given in [17] and [18].

The function $G(\theta)$ is dependent only on θ, in other words, $\omega_e t$, nothing else. That means, for any rotor speed or frequency, the value of $G(\theta)$ and the corresponding θ will be exactly the same. The relationship of $G(\theta)$ and θ is quite independent of rotor speed. If the rotor speed increases, the time t decreases in a way that the value $\omega_e t$ stays the same for corresponding $G(\theta)$.

So, the consequence of rotor speed decrease or increase is the G(θ) is to shrink or widen, but the shape remains same. As a result, if we can find the value of G(θ) somehow, the corresponding value of θ will be equal to $\tan^{-1} G(\theta)$, regardless of the speed. This observation allows the detection rotor position at any rotor speed and random noise of any peak value.

Irrespective of the speed, θ has a range of -90° to +90°, and commutation occurs at a point when θ changes from +90° to -90°. At every simulation instant, the value of $\omega_e t$ is saved in the form of tan^{-1} G (θ). When the value of $\tan^{-1} G(\theta)$ becomes ±90°, it is checked if the previous $\tan^{-1} G(\theta)$ value was the previous value of $\omega_e t$, which is chosen by the resolution set by the controller. If a noise of any value occurs at any point and offers a θ value which is equal to ±90°, the previous value of θ is checked and if the previous value is not 89° (a value slightly lower than 90^o), the value of 90° is rejected and commutation is not performed. If the previous value is 89°, then again the comparison is performed with a resolution of 0.1°. The concept is illustrated using the flow chart in Fig. 4-18.

So regardless of the noise amplitude, the commutation point can be accurately determined, unlike [17] and [18] where some threshold values have to be set for noise removal. Since the values of noise spikes are unknown, the values of thresholds have to be chosen carefully. In this method, there is no need to choose a threshold.

In order to illustrate the method further, two reference cases are discussed. One of them is when a noise occurs somewhere around θ = 50°, and the other case is when the noise occurs at θ > 89°.

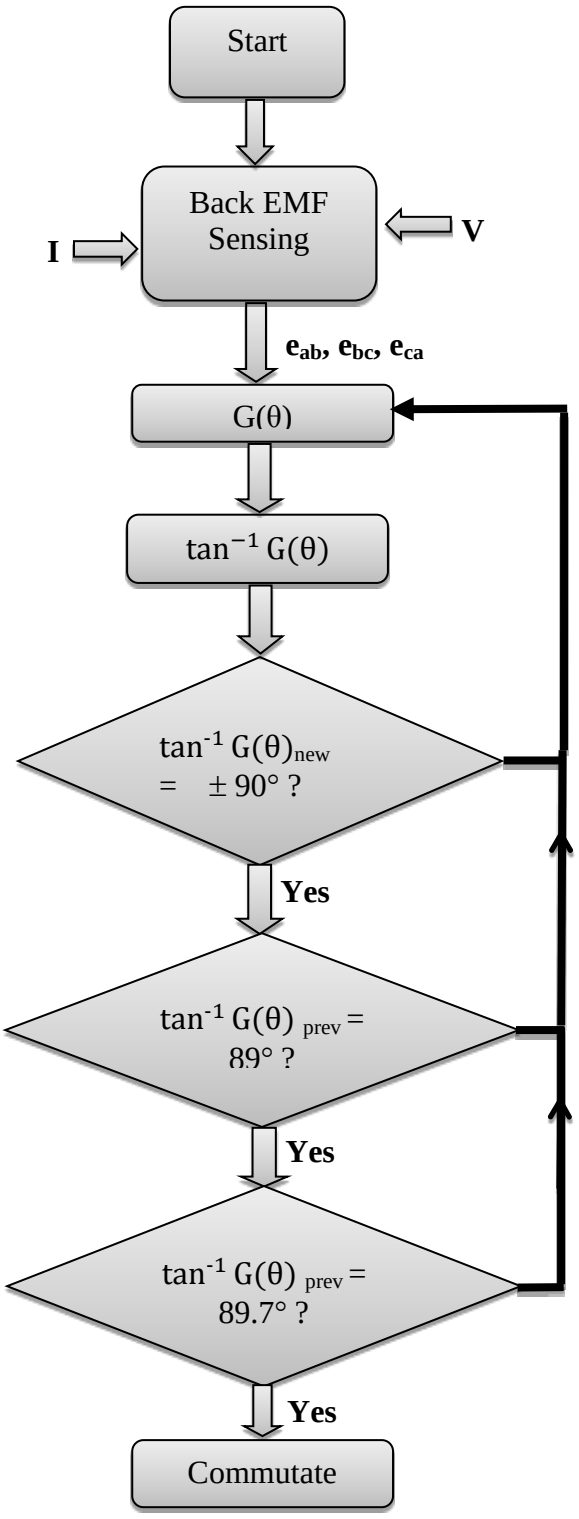

Fig. 4-18. Flow chart for illustrating the concept of the proposed commutation method

4.3.3. **Case Study 1: θ = 50°**

If a noise occurs when the speed of rotor is defined by $\theta = \omega_e t = 50°$ with a very high peak value, the value of $\frac{f_{bc}(\theta)}{f_{ab}(\theta)}$ will be equal to the set value and as a result, according to the conventional method, 50^o will be considered as the commutation instant. This scenario is illustrated in Fig. 4-19.

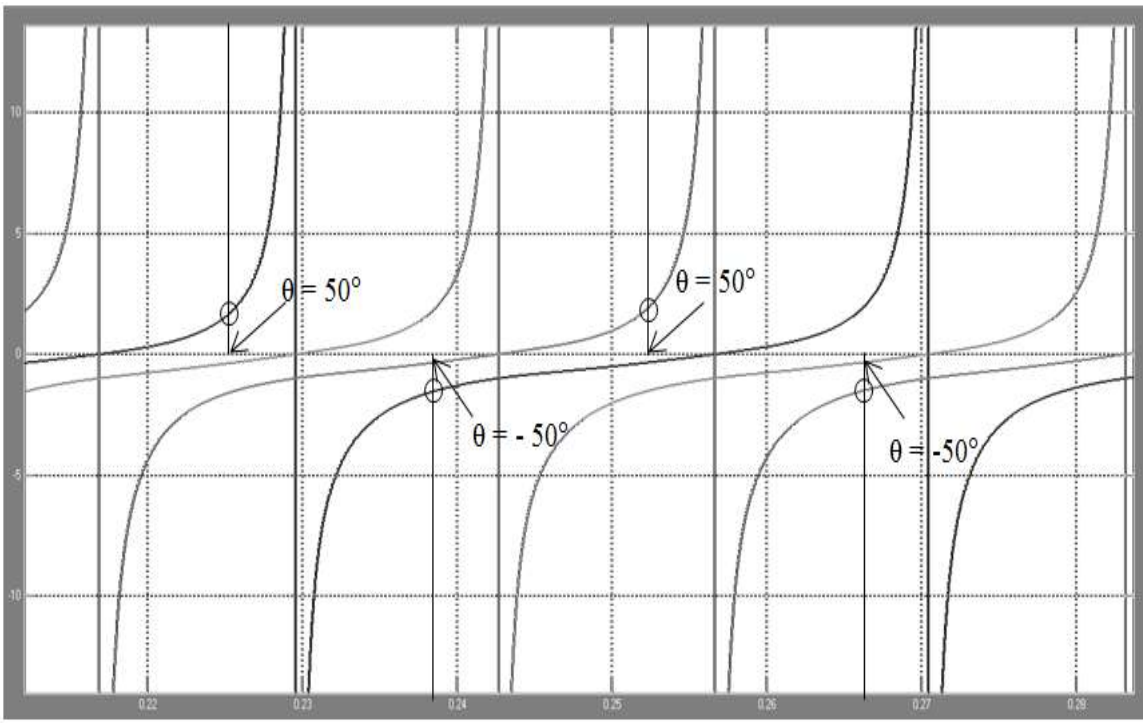

Fig. 4-19. Illustrating a noise signal in ±50° of commutation signal

According to the method proposed in this thesis, when the noise as shown in the Fig. 4-19 occurs, instead of considering the value of the noise (or any value), the value of $\theta = \tan^{-1} G(\theta)$ will be considered, which in this case, will be 90°. Instead of commutating instantly, the controller will compare the previous value of θ with 89°. Obviously, since the previous value is not 89°, the instant will be rejected as a commutation instant. In this way, any value of noise which comes

across the system before 89° will be rejected and no abrupt commutation will occur. Thus, the system will be protected.

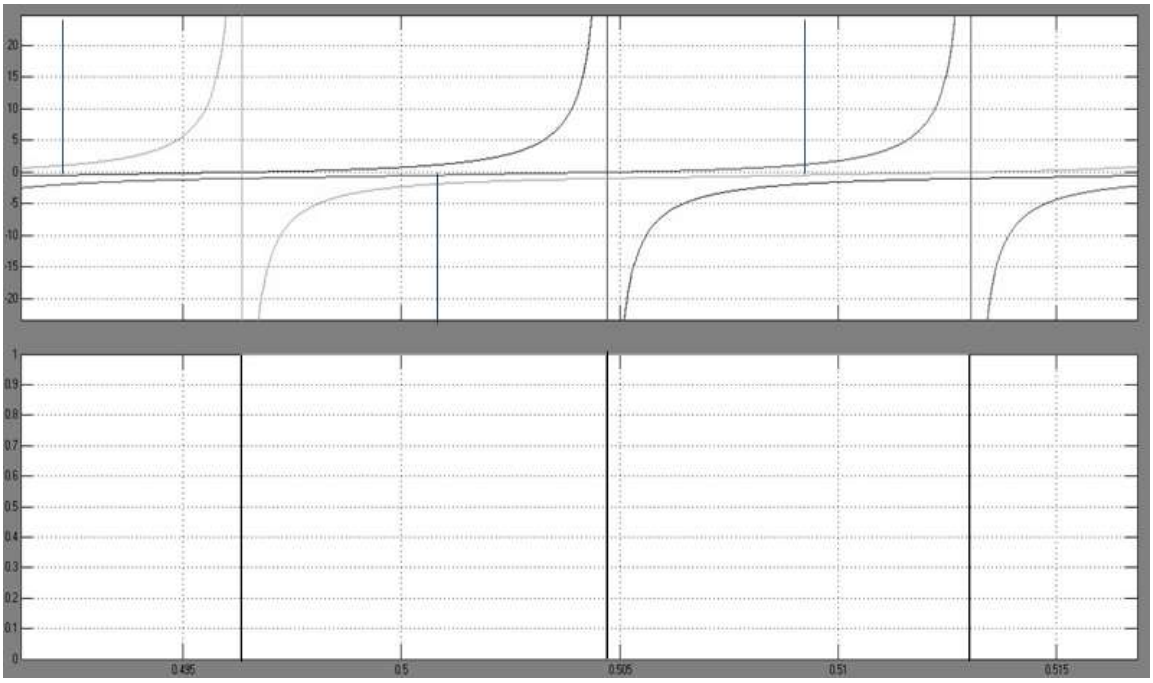

Fig. 4-20. Illustrating G(θ) with a noise in 50° and corresponding commutation signal with the proposed algorithm

4.3.4. **Case Study 2: θ = 89.3°**

If a noise occurs at an instant when rotor speed is defined by $\theta = \omega_e t = 89.3°$ which is very close to 90° but not exactly the commutation instant, the controller might consider it as a commutation instant due to the value of the noise. This scenario is illustrated in Fig. 4-21. In the method proposed in this thesis, the controller will calculate the value of $\theta = 89.3°$ and since the value is more than 89°, it will compare the value with 89.7°, which will turn out to be false, and the instant will not be considered as a commutation instant, as illustrated in Fig. 4-22.

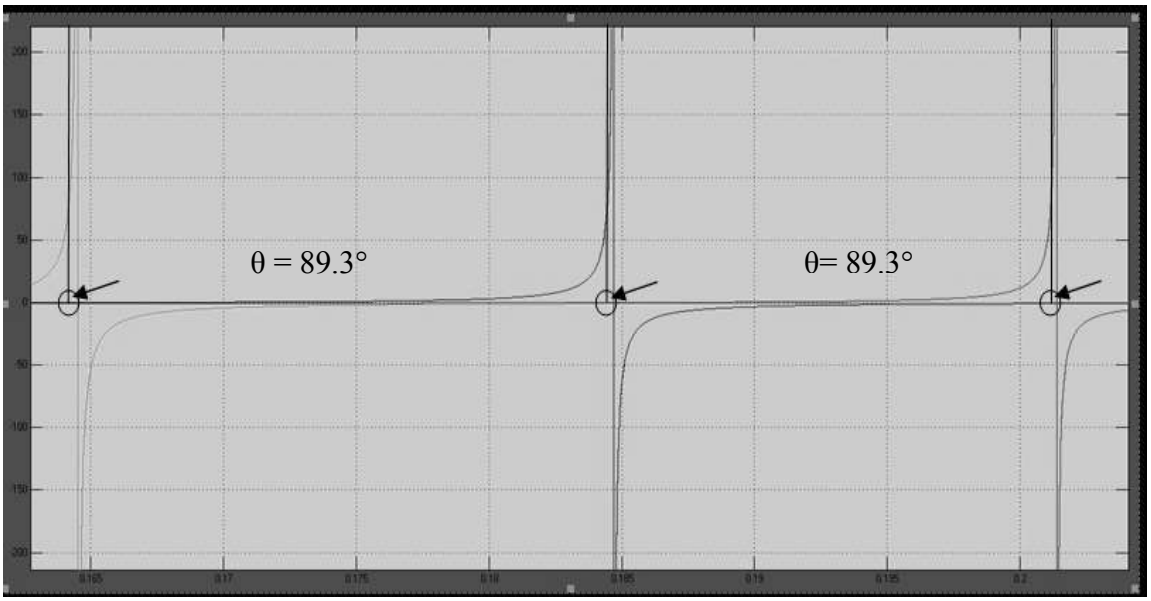

θ = 89.3°

Fig. 4-21. Expanding G(θ) with a noise signal at 89.3°

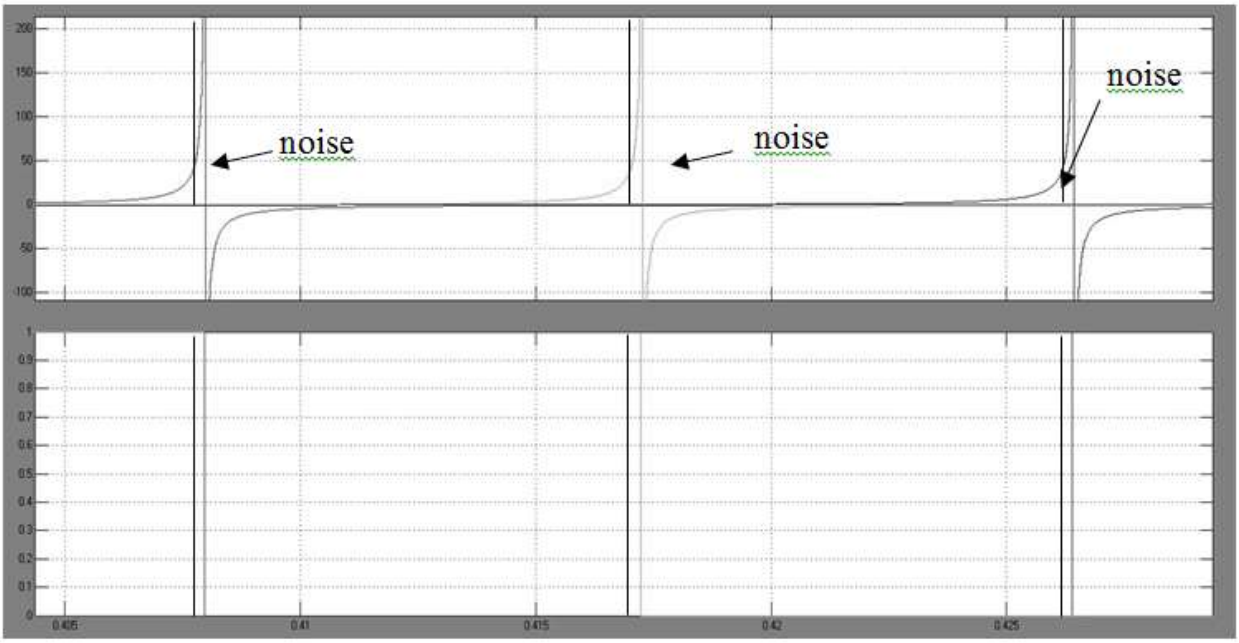

Fig. 4-22. Illustrating G(θ) with a noise at 89.3° and corresponding corrected commutation signal with the proposed method

Fig. 4-23 to Fig. 4-26 show a step input of 1500 RPM to 50 RPM and the corresponding speed response along with other functions.

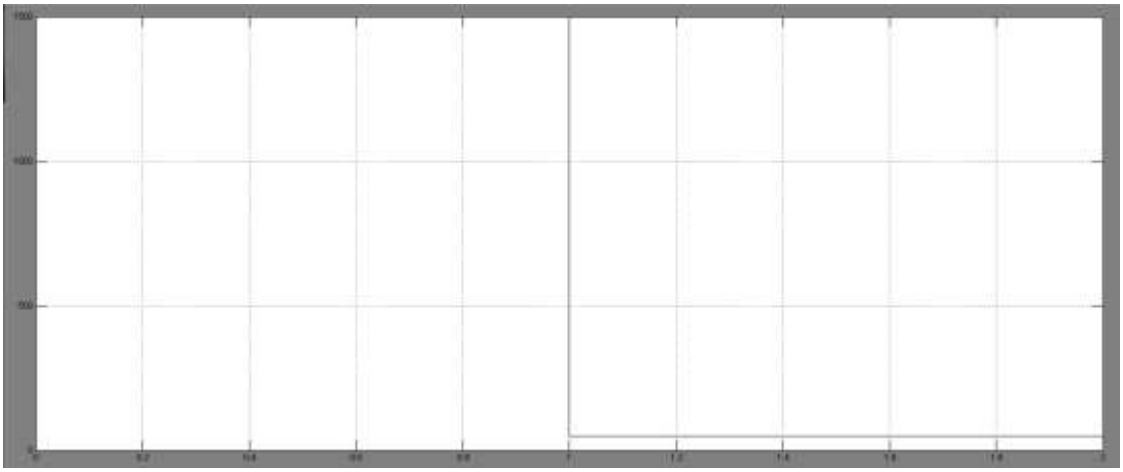

Fig. 4-23. Step speed input from 1500 RPM to 50 RPM

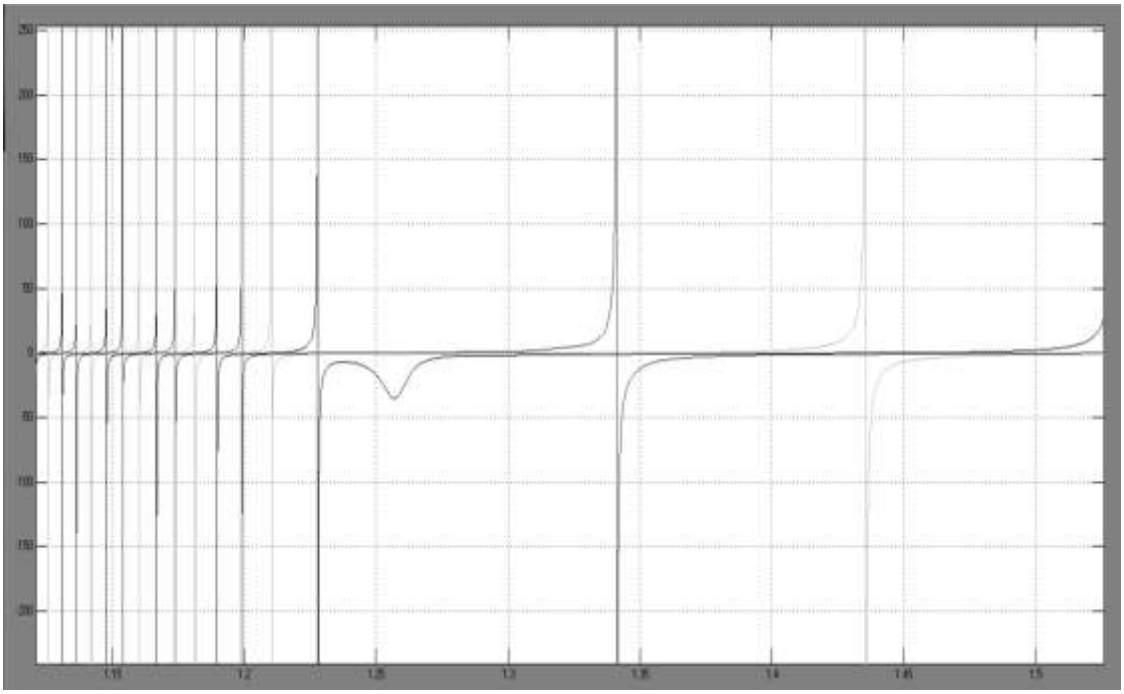

Fig. 4-24. Plot of G(θ) function

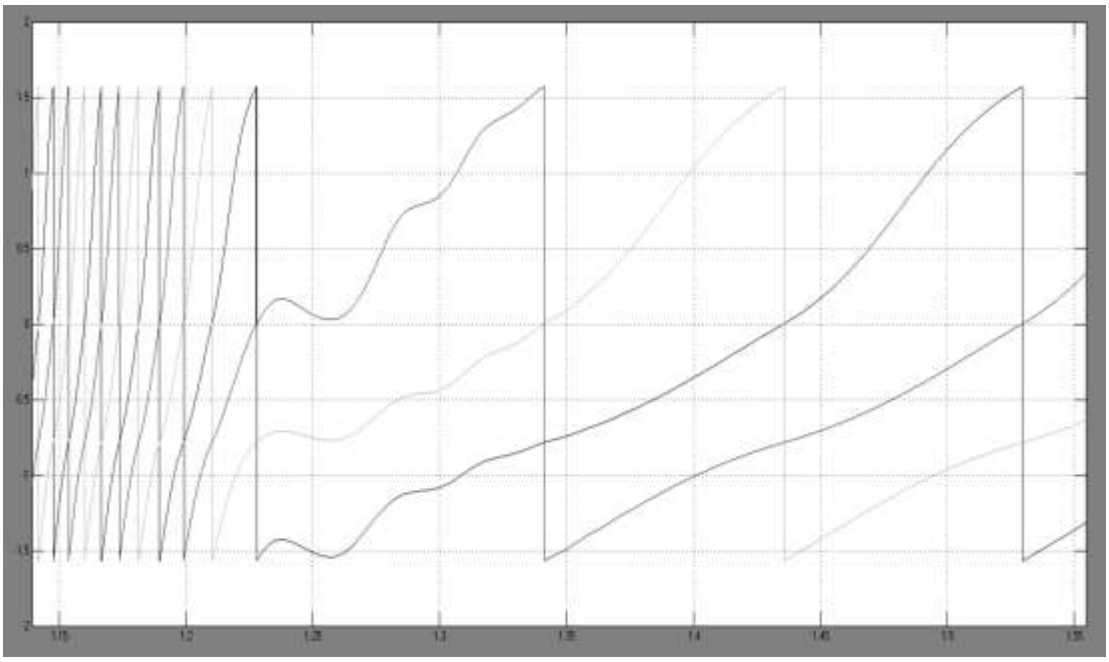

Fig. 4-25. Plot of $\theta = \tan^{-1} G(\theta)$

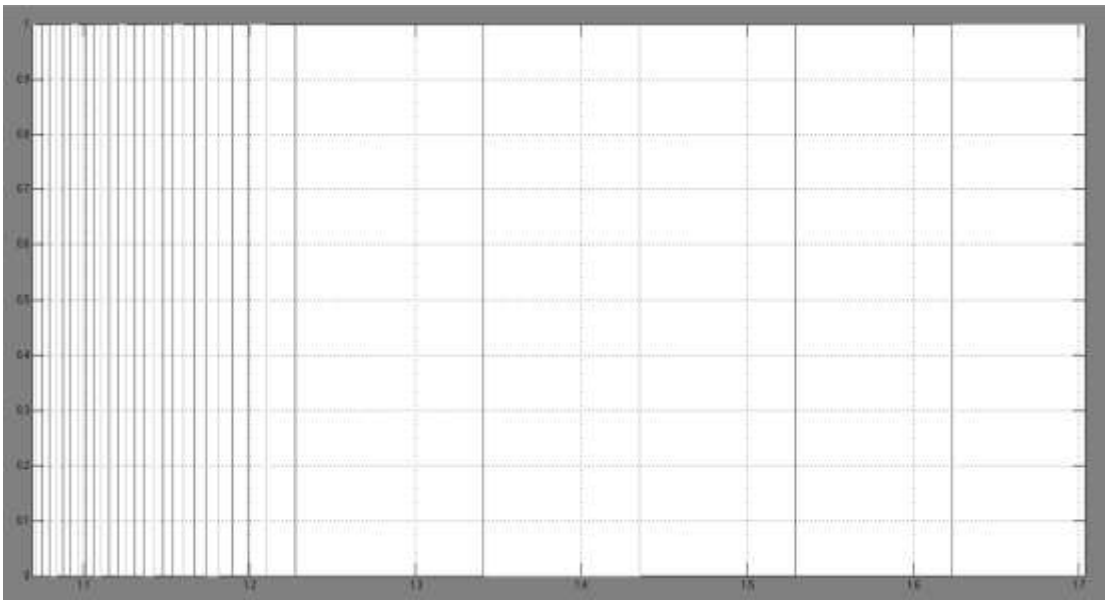

Fig. 4-26. Commutation pulses from $\theta = \tan^{-1} G(\theta)$

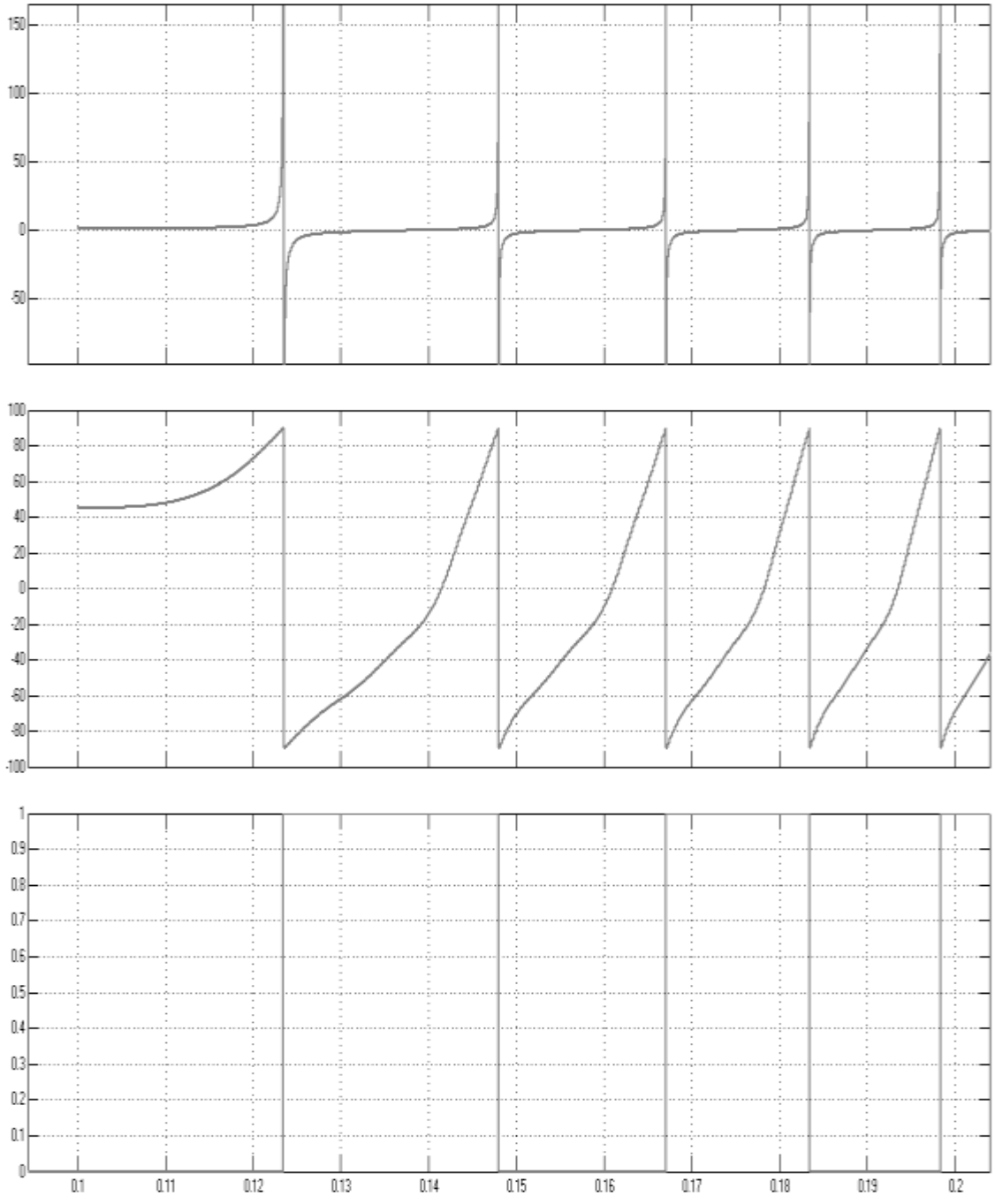

Fig. 4-27. $G(\theta)$, $\theta = \tan^{-1} G(\theta)$ and commutation signal in one frame

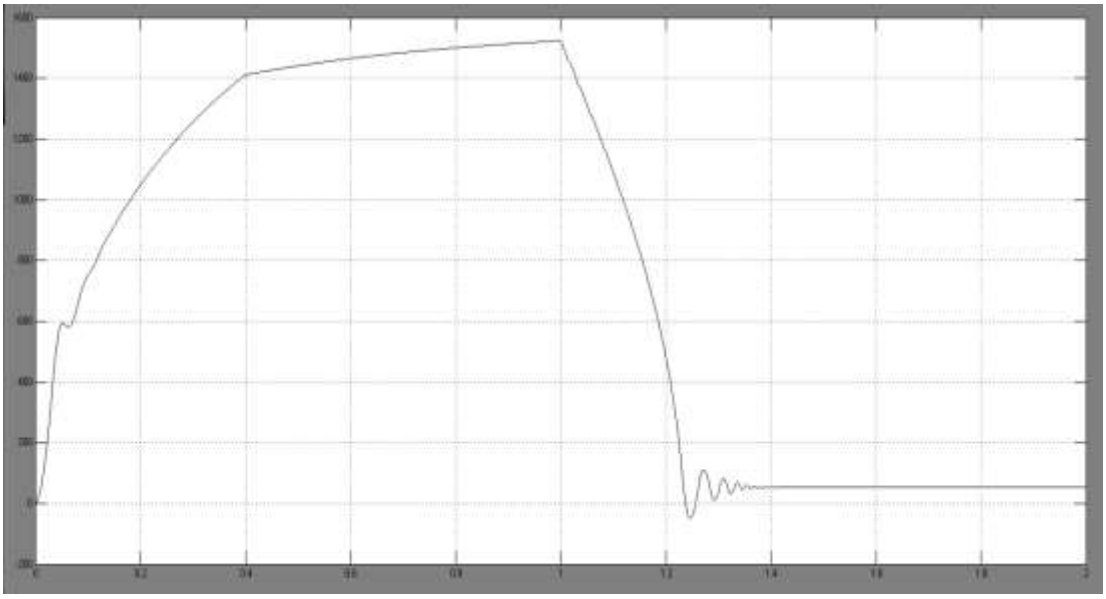

Fig. 4-28. Speed Response

4.4. Conclusion

In this chapter, an improved algorithm for sensorless BLDC motor control is described with illustration, appropriate simulation results and proof of concept. Conventional sensorless motor control schemes are discussed in detail with their advantages and disadvantages. The basis for the method described in this thesis is established through mathematical modeling and proof. A completely noise independent commutation scheme which is an improvement over the previous scheme [18] is discussed along with simulation results.

CHAPTER 5. CONCLUSION

5.1. Summary of Work Done

The application of Brushless DC motors has grown significantly in recent years, especially in the field of home appliances and automotive industry. BLDC motor is a good choice in these fields due to their ruggedness, compactness, low cost and low maintenance. Prime challenges of a BLDC driven system are to keep the cost low with high level of reliability and efficiency. BLDC drives with sensors are adequate to control speed over a wide range. The position sensors used in this control are good for accurate position information needed for speed control. But they have the diadvantages of high cost and poor reliability.

Sensorless control systems overcome some of the limitations of sensor-ed control systems. They are typically cheaper. Although a significant number of sensorless control schemes have been proposed, none of them are quite good in terms of accuracy and reliability. Their operation in the low speed range is not satisfactory, and noise coming from the surrounding makes these systems unreliable.

In this paper, an improvement of the state observer based method of BLDC control system over the one proposed in [18] has been presented. This method is noise free and will not affect the commutation cycle or processing speed. Simulation results to support this method are presented. The proposed method avoids using a virtual neutral point for back EMF sensing [8] and threshold in speed independent commutation functions [18] and [17]. Instead, this method uses electrical angle corresponding to the commutation function value, which is a novel method and works for any level of noise, which makes the system robust and durable.

5.2. Future Research

The proposed tangent function based algorithm is simulated in Simulink and verified. Since it cannot be used in industrially unless it is implemented with a real time aptitude, the next step will be to implement it with a suitable microcontroller or digital signal processor.

One specific application of BLDC motor is in the field of racing car. Industrial racing toy cars use BLDC motors which can run up to 60000 RPM. In order to implement a sensorless speed control scheme in this particular application, some special microcontrollers have to be used. The microcontroller has to be of low cost, powerful enough to handle the processing of algorithm and have all necessary peripherals. It has to have ADC to take current and speed as inputs, timer with PWM generation capability etc.

A very convenient microcontroller for this application with low cost is STMicroelectronics STM32FO51R8. It has 32 bit ARM cortex processor with upto 48 MHz clock speed, SPI, I^2C and UART communication for less than a dollar price. The next step of this thesis is to implement the proposed sensorless speed control algorithm in racing car application with STM32 microcontroller.

REFEREN CES

[1] B. L. Theraja, “A Textbook of Electrical Technology", (Volume II) .

[2] Thomas Kaporch, “Driving the Future.pdf.”, Appliance Manufacture, Sept.2001, pp. 43-46.

[3] J.-S. Park, B.-G. Gu, J.-H. Choi, and I.-S. Jung, “Development of BLDC Motor Drive for Automotive Water Pump Systems,” *Journal of International Council on Electrical Engineering*, vol. 1, no. 4, pp. 395–399, Oct. 2011.

[4] R. Krishnan, *Permanent Magnet Synchronous and Brushless DC Motor Drives*. 2010, Francis Group.

[5] Jianwen Shao, “Direct Back EMF Detection Method for Sensorless Brushless DC (BLDC) Motor Drives," Master's Thesis submitted to the Faculty of the Virginia Polytechnic Institute and the State University, 2003.

[6] G. Su, S. Member, and J. W. Mckeever, “Low-Cost Sensorless Control of Brushless DC Motors With Improved Speed Range,” vol. 19, no. 2, pp. 296–302, 2004.

[7] J. S. J. Shao, D. Nolan, and T. Hopkins, “Further improvement of direct back EMF detection for sensorless brushless DC (BLDC) motor drives,” *APEC Seventeenth Annual IEEE Applied Power Electronics Conference and Exposition Cat No02CH37335*, vol. 2, no. c, pp. 33–38, 2002.

[8] K. Iizuka, H. Uzuhashi, M. Kano, T. Endo, and K. Mohri, “Microcomputer Control for Sensorless Brushless Motor ri,” vol. I, no. 4, pp. 595–601, 1985.

[9] J. G. Moreira, “Indirect sensing for rotor flux position of permanent magnet ac motors operating in a wide speed range,", *IEEE Trans. Ind. Applicat.*, vol. 32, pp. 401–407, Nov./Dec. 1996.

[10] R. C. Becerra, T. M. Jahns, and M. Ehsani, “Four-quadrant sensorless brushless ECM drive,” in *Proc. IEEE APEC’91 Conf.*, 1991, pp. 202–209.

[11] T. M. Jahns, R. C. Becerra, M. Ehsani, and S. Member, “Integrated Current Regulation for a Brushless ECM Drive,” vol. 6, no. I, pp. 118–126, 1991.

[12] N. Ertugrul and P. Acarnley,“ A new algorithm for sensorless operation of permanent magnet motors” vol. 30, no. 1, pp. 126–133, 1994.

[13] R. Wu and G. R. Slemon, “A Permanent Magnet Motor Drive Without a Shaft Sensor,” vol. 21, no. 5, 1991.

[14] S. Ogasawara and H. Akagi, “An approach to position sensorless drive for brushless DC motors,” *IEEE Transactions on Industry Applications*, vol. 27, no. 5, pp. 928–933, 1991.

[15] P. B. Machines, J. X. Shen, S. Member, Z. Q. Zhu, and D. Howe, “Sensorless Flux-Weakening Control of Using Third Harmonic Back EMF,” vol. 40, no. 6, pp. 1629–1636, 2004.

[16] S. B. Ozturk and H. a. Toliyat, “Direct Torque and Indirect Flux Control of Brushless DC Motor,” *IEEE/ASME Transactions on Mechatronics*, vol. 16, no. 2, pp. 351–360, Apr. 2011.

[17] T.-H. K. T.-H. Kim and M. Ehsani, “Sensorless control of the BLDC motors from near-zero to high speeds,” *IEEE Transactions on Power Electronics*, vol. 19, no. 6, pp. 1635–1645, 2004.

[18] T. Kim, B. Park, D. Lee, J. Ryu, and D. Hyun, “A New Approach to Sensorless Control Method for Brushless DC Motors,” *International Journal*, vol. 6, no. 4, pp. 477–487, 2008.

[19] a. T. Alexandridis and G. D. Galanos, “Design of an optimal current regulator for weak AC/DC systems using Kalman filtering in the presence of unknown inputs,” *IEE Proceedings C Generation, Transmission and Distribution*, vol. 136, no. 2, p. 57, 1989.

[20] M. Saif, “Robust servo design with applications,” *IEE Proceedings D Control Theory and Applications*, vol. 140, no. 2, p. 87, 1993.

[21] J. F. Marsh and M. Aldeen, “Decentralised observer-based control scheme for interconnected dynamical systems with unknown inputs,” *IEE Proceedings - Control Theory and Applications*, vol. 146, no. 5, pp. 349–358, Sep. 1999.

[22] Shane W. Colton, “Design and Prototyping Methods for Brushless Motors and Motor Control” Master's thesis submitted to the graduate faculty of massachusetts Institute of Technology, 2010.

[23] R. Krishnan, “*Electric Motor Drives*”, Prentice Hall.

[24] Stefán Baldursson, “BLDC Motor Modelling and Control – A Matlab ® /Simulink ® Implementation ,” Master's Thesis submitted to the graduate faculty of Chalmars University, 2005.

[25] P. Kshirsagar, U. Technologies, E. Hartford, and V. Tech, “High Efficiency Current Excitation Strategy for Variable Speed Non- Sinusoidal Back-EMF PMSM Machines,” no. c, 2011.

[26] I. Colak and M. Sahin, “Sensorless Control of a Brushless DC Motor Using a Self-Tuning PID,” pp. 1057–1062, 2012.

[27] M. Demirtas, “Off-line tuning of a PI speed controller for a permanent magnet brushless DC motor using DSP,” *Energy Conversion and Management*, vol. 52, no. 1, pp. 264–273, Jan. 2011.

[28] Q. Jiang, C. Bi, and R. Huang, “A new phase-delay-free method to detect back EMF zero-crossing points for sensorless control of spindle motors,” *IEEE Transactions on Magnetics*, vol. 41, no. 7, pp. 2287–2294, Jul. 2005.

[29] V. G. T. K, M. T. Student, and S. T. George, “DSP based Speed Control of Permanent Magnet Brushless DC Motor,” pp. 50–55, 2011.

[30] J. Gao and Y. Hu, “Direct Self-Control for BLDC Motor Drives Based on Three-Dimensional Coordinate System,” *IEEE Transactions on Industrial Electronics*, vol. 57, no. 8, pp. 2836–2844, Aug. 2010.

[31] Y.-S. Lai and Y.-K. Lin, “A Unified Approach to Zero-Crossing Point Detection of Back EMF for Brushless DC Motor Drives without Current and Hall Sensors,” *IEEE Transactions on Power Electronics*, vol. 26, no. 6, pp. 1704–1713, Jun. 2011.

[32] J. Böcker, “Advanced Hysteresis Control of Brushless DC Motors.”, www.boecker-engineering.de.

[33] A. Rubaai, M. Ieee, D. Ricketts, M. D. Kankam, and S. Member, “Development and Implementation of an Adaptive Fuzzy-Neural-Network Controller for Brushless Drives,” vol. 38, no. 2, pp. 441–447, 2002.

[34] C. Pan, E. Fang, and S. Member, “A Phase-Locked-Loop-Assisted Internal Model Adjustable-Speed Controller for BLDC Motors,” vol. 55, no. 9, pp. 3415–3425, 2008.

[35] C. S. Joice, S. R. Paranjothi, and V. J. S. Kumar, “Digital Control Strategy for Four Quadrant Operation of Three Phase BLDC Motor With Load Variations,” *IEEE Transactions on Industrial Informatics*, vol. 9, no. 2, pp. 974–982, May 2013.

[36] J. Shi and T.-C. Li, “New Method to Eliminate Commutation Torque Ripple of Brushless DC Motor With Minimum Commutation Time,” *IEEE Transactions on Industrial Electronics*, vol. 60, no. 6, pp. 2139–2146, Jun. 2013.

[37] F. Aghili and S. Member, “Fault-Tolerant Torque Control of BLDC Motors,” vol. 26, no. 2, pp. 355–363, 2011.

[38] M. P. Kazmierkowski, L. G. Franquelo, J. Rodriguez, A. Perez, and J. I. Leon, “Development of New Converter Topologies,” IEEE Industrial Electroincs Magazine, pp. 6–26, september, 2011.

[39] D. Grenier, L. Dessaint, S. Member, O. Akhrif, Y. Bonnassieux, and B. Le Pioufle, “Experimental Nonlinear Torque Control of a Permanent-Magnet Synchronous Motor Using Saliency,” vol. 44, no. 5, pp. 680–687, 1997.

[40] A. H. Niasar, A. Vahedi, and H. Moghbelli, “Speed Control of a Brushless DC Motor Drive via Adaptive Neuro-Fuzzy Controller Based on Emotional Learning Algorithm dt Bo) r,” pp. 230–234.

[41] D. Jung and I. Ha, “Low-cost sensorless control of brushless DC motors using a frequency-independent phase shifter,” *IEEE Transactions on Power Electronics*, vol. 15, no. 4, pp. 744–752, Jul. 2000.

[42] J. Park, S. Member, and S. Jung, “Design and Analysis of P19

osition Tracking Observer Based on Instantaneous Power for Sensorless Drive of Permanent Magnet Synchronous Motor," vol. 27, no. 5, pp. 2585–2594, 2012.

[43] H. Yeo, C. Hong, J. Yoo, and A. S. Korca, "Sensorless Drive for Interior Permanent Magnet Brushless DC motors," pp. 5–7, 1997.

[44] C. B. Rasmussen and E. Ritchie, "VARIABLE SPEED BRUSHLESS DC MOTOR DRIVE FOR HOUSEHOLD REFRIGERATOR COMPRESSOR C. B. Rasmussen, E. Ritchie Aalborg University, Denmark," no. 444, pp. 128–132, 1997.

[45] B. Marx, D. Koenig, and J. Ragot, "Design of observers for Takagi – Sugeno descriptor systems with unknown inputs and application to fault diagnosis."